energies

Article

Performance of Linear Generator Designs for Direct Drive Wave Energy Converter under Unidirectional Long-Crested Random Waves

Budi Azhari [1], Fransisco Danang Wijaya [2,*] and Edwar Yazid [1]

[1] Research Center for Electrical Power and Mechatronics, Indonesian Institute of Sciences, Jl. Sangkuriang, Dago, Bandung 40135, Indonesia; budi.azhari19@gmail.com (B.A.); edwar.putra@gmail.com (E.Y.)
[2] Department of Electrical Engineering and Information Technology, Universitas Gadjah Mada, Jl. Grafika, Sleman, Yogyakarta 55281, Indonesia
* Correspondence: danangwijaya@ugm.ac.id

Abstract: For generating electricity, direct-drive wave energy converters (WECs) with linear permanent magnet generators (LPMGs) have advantages in terms of efficiency, simplicity, and force-to-weight ratio over WEC with rotary generators. However, the converter's work under approaching-real wave conditions should be investigated. This paper studies the performance of a pico-scale WEC with two different LPMGs under unidirectional long-crested random waves. Different significant wave heights (using data in the Southern Ocean of Yogyakarta, Indonesia) and peak frequencies are tested. The JONSWAP energy spectrum is used to extract the wave elevations, while the MSS toolbox in MATLAB Simulink is employed to solve the floater's dynamic responses. Next, the translator movements are extracted and combined with the flux distribution from FEMM simulation and analytical calculation, and the output powers are obtained. An experiment is conducted to test the output under constant speed. The results show for both designs, different tested significant wave height values produce higher output powers than peak frequency variation, but there is no specific trend on them. Meanwhile, the peak frequency is inversely proportional to the output power. Elimination of the non-facing events results in increasing output power under both parameters' variation, with higher significant wave height resulting in a bigger increase. The semi iron-cored LPMG produces lower power loss and higher efficiency.

Keywords: iron-cored; semi iron-cored; LPMG; significant wave height; peak frequency; random wave; output power

check for updates

Citation: Azhari, B.; Wijaya, F.D.; Yazid, E. Performance of Linear Generator Designs for Direct Drive Wave Energy Converter under Unidirectional Long-Crested Random Waves. *Energies* **2021**, *14*, 5098. https://doi.org/10.3390/en14165098

Academic Editor: Eugen Rusu

Received: 8 June 2021
Accepted: 20 July 2021
Published: 18 August 2021

1. Introduction

Ocean waves in the world have been known to reserve a significant amount of energy that can be utilized for generating electricity. It is estimated that the global potential energy of this resource reaches up to 1170 TWh in a year [1]. Compared to other renewable energies, wave energy has a larger energy density [2]. Some reports show that in terms of power density, an average of 2–3 kW/m^2 power can be harnessed from a wavefront compared to 1.366 kW/m^2 of the average global solar irradiance and 0.6 kW/m^2 from wind farms [3–5]. Ocean energy is also more concentrated, more predictable, and more persistent than other renewable resources; also, it is more frequent, as it is available all the time regardless of the weather and climate [3,4,6]. The vast distribution is another advantage, as the ocean is covering about two-thirds of the planet's surface.

However, some data show that the contribution of wave energy converter (WEC) in electricity generation is still relatively low, although development is continuously performed. In 2019, the total installed WEC capacity across Europe is 11.8 MW, including a 25% of increase in capacity compared to the previous year [7]. China, one of the most energy-consumptive countries, has also intensified its development. As of 2017, there were

49 WEC projects conducted. Some tens of them have the capacity of more than 100 kW, while the remaining ones produce lower output power [8]. Meanwhile, the data from the end of 2016 show that the total WEC capacity in North American countries was still around 2.07 MW, including those that were in the planning stage [9]. Considering these numbers, there is still big room for improvement, research, and development to increase the WEC share in electricity generation. The list of completed and ongoing projects around the world can be found in [7–10].

Indonesia, as the largest archipelagic country, can also benefit from the WEC deployment. It has one of the longest coastal lines in the world; some areas have an average wave height of more than 2 m [11]. Thus, a lot of potential sites can be exploited. It is estimated that the WEC utilization in Indonesia can produce around 18 GW of electricity [12], which is equivalent to 27.7% of the total generated power in 2018 [13]. For this reason, researchers have made feasibility studies, assessing potential places for the WEC deployment [14–18]. The next step, the design of a specific WEC system to be placed in a certain site, needs to be investigated and detailed. The study of the system's operation under varying real wave conditions is also required. This paper will take part in the last stage, focusing on the work of a WEC system under random wave scenarios in Indonesia.

So far, the WEC itself has had a wide variety of models. Since the technology is relatively new, many studies and projects have come up with different proposed models. They can be differentiated based on many criteria such as operating principle, converter motion, power take-off method, mechanical structure, placement location, etc. [19,20]. However, one good classification to summarize its development from the beginning is according to the converter motion.

Initially, conventional WECs work by capturing the wave motion and then converting it to the suitable movement of rotating generators through gearboxes, screws, hydraulic devices, or turbines. Some models exercising this principle including oscillating water columns (as applied in Shangwei, China since 2000, Mutriku, Spain in 2011, and Oceanlinx in Australia in 2013) [21], overtopping devices (as applied in WaveDragon in Denmark in 2003) [22], and flexible membranes (as applied in the Bombora project in Australia in 2012) [23]. In 2004, the Indonesian government also had built a pilot WEC project using an oscillating water column on the southern coast of Java Island [24].

Nevertheless, the work of those devices has a major drawback as the mechanical efficiency decreases with the presence of intermediary motion converters. Alternatively, direct-drive conversion by employing a linear permanent magnet generator (LPMG) has been introduced. It is estimated that around 30% of the existing projects around the world are utilizing this model, second to 42% of the conventional model with hydraulic use [25]. The direct-drive scheme is proven to result in the highest efficiency among all WECs [26,27]. As shown in Figure 1, the conventional WEC undergoes several stages before producing electricity; with each stage is dissipating loss [28]. In LPMG-driven WEC, the linear movement of its translator is in accordance with the wave heave motion; thus, the intermediaries can be eliminated, and the losses can be minimized. Other advantages including less maintenance and a high force-to-weight ratio [29,30]. The use of permanent magnets in LPMG also brings simpler construction yet high flux density [31]. Excellent reviews related to the WEC using LPMG can be found in [32,33].

Regarding the LPMG, it also has several developed models. Based on the basic shape, there are tubular and flat LPMG. In the first model, the device is formed into a hollow cylinder body. It has a uniform air gap; thus, it results in a smaller cogging force, no transverse edge effect, and lower manufacturing cost [34–36]. Meanwhile, the flat model forms a hollow prism device; the top and the base can be rectangular or triangular [37]. In a comparative study, the triangular shape was known to produce better electromagnetic characteristics than the rectangular one [38]. Meanwhile, Oprea et al. [39] concluded that the flat type results in similar coil flux magnitude and induced voltage to the tubular one, but it is favorable in terms of manufacturing ease.

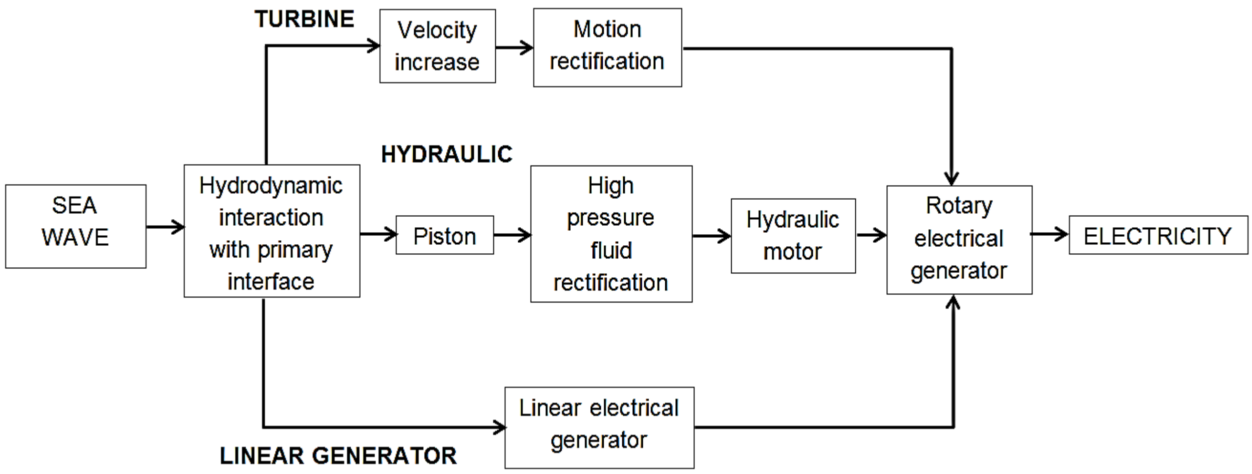

Figure 1. Working process of different WEC types.

Some variations have also been developed regarding the filling materials. First, the conventional iron-cored LPMG is composed of ferromagnetic-based laminations in its stator [35,37]. Having benefited from low reluctance and high flux density, it also suffers from high ripple caused by significant cogging force. Alternatively, air-cored LPMG is developed, which consists of no ferromagnetic part in its body. The design is proposed, among others by Vermaak et al. [40]. Trapezoidal permanent magnets are assembled on the translator's teeth; the teeth come out as radial branches of the translator cylindrical core sheet. Thus, pair-wise flux coupling between adjacent magnets that result in attractive forces can be avoided. In another design, Brovont et al. [41] integrated an air-cored LPMG into a mobile water quality sensor. The magnets moved along a 38.3 mm column and produced 0.4 V output voltages. Basically, the air-cored type can eliminate the cogging force. However, the nonexistence of ferromagnetic material will drastically increase the reluctance as well as drop the air gap flux density and the windings' flux linkage. To avoid a significant decrease in the electrical output, compensations have to be made.

Previously, accommodative actions have been taken to present an LPMG with less cogging force but still maintaining the electrical output. In semi iron-cored LPMG [42], the idea was to make some eliminations in the iron material on several parts. The decrease of the flux linkage in the stator winding was anticipated by adjusting the number of winding turns. The resulted copper loss eventually increases, but core loss, as well as mechanical loss from the cogging force, can be minimized. The overall loss assessment showed that this innovation can produce better efficiency compared to the conventional design. Still, manufacturing this design is more difficult, as the stator body is neither in an integrated nor compact shape.

From the explanation, it can be deduced that the direct-drive system with LPMG as the converter is considered superior mainly in terms of conversion efficiency. Meanwhile, the LPMG can be selected from different models depending on which parameter will be the focus. Beforehand, some studies have proposed different LPMG models for direct-drive WEC [42,43] in Indonesia. The designs have even been optimized [43] and tested under wave conditions at the placement spot [44]. However, the wave operations that drive the WEC were simplified into regular conditions, of which the wave particles are assumed to move sinusoidally. Practically, this modeling has not been sufficient enough either for representing the real wave dynamics or testing the WEC system.

To make a more valid assessment of the WEC performance and to better understand the influences of different wave parameters on the WEC outputs, the converter system should be operated in approaching-real wave conditions. In this paper, the performance of the two different LPMGs will be investigated under unidirectional long-crested random waves, with the case study in the Southern Ocean of Yogyakarta, Indonesia. In running the wave scenarios, different significant wave height values are applied. To make a credible assessment, the real wave height data in the designated placement location are used. The peak frequency of the wave is also varied, using some selected values. Then, the output profiles of both LPMGs are extracted through several processes, which include the simulation using MATLAB Simulink and finite element magnetic-based software of FEMM as well as analytical calculation. From the results, the relation between different wave parameters and design aspects of the LPMGs can be explored. The influences of different random wave parameters on the WEC outputs can also be known. These pieces of information are significant for improving the current designs or proposing different ones. Furthermore, a comparison between the two LPMG configurations can be assessed based on their respective outputs. Then, the assessment can be used to evaluate the advantages of each model to be applied in the designated location.

2. Design Concept and System Modeling

The LPMGs are utilized for a direct-drive WEC system, wherein mechanical energy is directly converted into electricity. In this concept, the WEC system is stationed in open water, as depicted in Figure 2. It consists of two main components: the floater and the power converter. The former functions as the wave's mechanical energy capturer while the latter converts the mechanical energy into electrical energy. Both parts are interconnected. They will be explained subsequently in the next subsections.

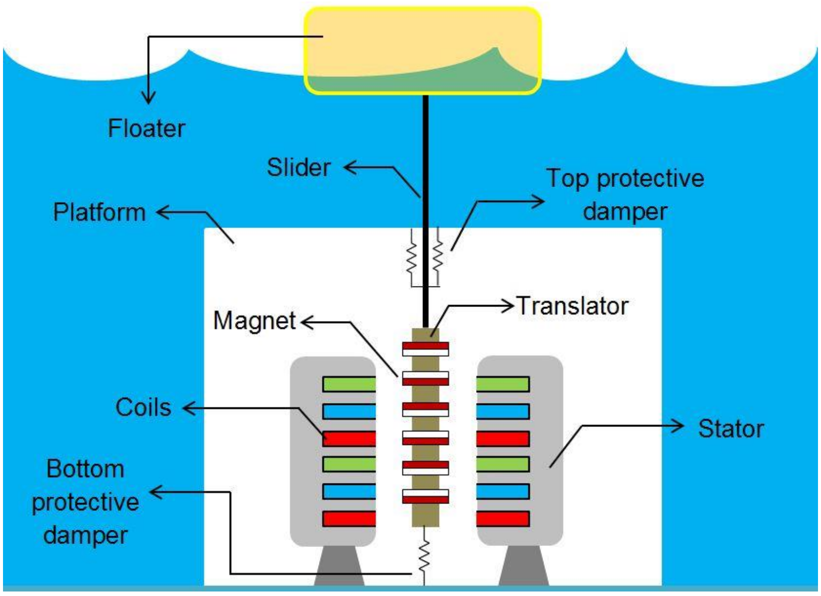

Figure 2. Placement of the proposed direct-drive WEC.

2.1. Design Concept of the WEC

The floater forms a single cylindrical body whose diameter can be set based on the system capacity. It has a smaller density than the sea water, so it can float and move freely according to the incoming waves. In reality, the floater can have six degrees of freedom (DoF), as its motion in any direction will move the converter's moving part, inducing an electromagnetic process to generate electricity. The floater displacements represent the mechanical energies that work on it. Based on the floater's size compared to the incoming wavelength, the system is considered as a point absorber one, meaning that the floater diameter is considerably much smaller than the wavefront length. This model is the most widely used system in currently running converters [21]. To increase the power conversion rate, several points of WEC can be installed collectively in several spots. Then, the power captured by the floater can be approached by using the following Equation [45]

$$\frac{P_{capt}}{P_{mcl}} = d_f. \tag{1}$$

P_{capt} and P_{mcl} are the amount of power captured by the floater and power generated per meter of wave's crest length, both in watts. Meanwhile, d_f is the floater diameter (m).

Meanwhile, the proposed LPMG is a pico-scale (1 kW-rated) tubular permanent magnet excitation with a moving magnets setting. In this case, two different designs of linear PM generators will be operated and tested sequentially connected to the floater system. The LPMG is positioned inside a special platform that is attached to the seabed. It consists of two main components: the translator and the stator. The stator is fixed on the platform foundation, while the platform dimension is determined to enable the free movement of the translator according to the maximum wave height. To achieve it, a slider links the LPMG's translator to the floater. From the translator end, it stretches along the vertical axis and passes through the structure gateway. The gateway itself is a fixed doorway on the top of the structure. It functions to fix the translator movement and to minimize contact between the translator and seawater. The platform also has a protective function, as it should be able to withstand any dynamic forces from its environment, such as the deep water stream. It should also have a good resistance toward the water's salinity. These properties are meant to ensure the proper work of the generator.

As the inner component of the LPMG, the translator can move vertically, and its movement is proportional to the floater's motion. It has a core in its inner part, and a permanent magnet array as the excitation source is mounted on its outer part, encircling the core. The use of permanent magnets is simpler and more mechanically stable than the DC-current excitation system. In this design, the magnets are made of Neodymium-Iron-Boron (NdFeB) material of N40 type. They are arranged axially (Figure 3), in which two adjacent magnets have opposite magnetic orientations. A similar setting has been applied by Kim et al. (2017) [46], who preferred such an arrangement because of its low cost and easiness to configure. A tiny air gap separated the two adjacent magnets to reduce the pair-wise magnetic coupling effect. Furthermore, the translator stroke (movement range) is designed to equal the wave height variation by managing the distance between the top and bottom of the structure. On the top and bottom ends of the structure, protective dampers are installed to minimize the impact of collision when the translator reaches either end (Figure 2).

Figure 3. Axial magnet configurations.

On the other hand, the stator is kept rigidly and is positioned in the outer part of the LPMG, surrounding the translator. Its core has a cylindrical shape while the material filling of the core is differentiated based on the model: iron-cored or semi iron-cored. Both designs are shown in Figure 4, while the complete dimensions of all parts are tabulated in Table 1. In this design, the translator has a nearly equal length as the stator. Moreover, the stator has several slots, and three-phase windings are wound on them. The placement on the rigid stator provides mechanical stability and avoids any damaging friction to the coil. The following subsections describe each LPMG type sequentially.

2.1.1. Iron-Cored LPMG

The iron-cored model has ferromagnetic materials filling the whole stator body. As shown in Figure 4a, the teeth are radially inward extensions of the stator yoke. The dimensions of the stator parts are determined based on the expected output, and the use of a full ferromagnetic stator is also a consideration.

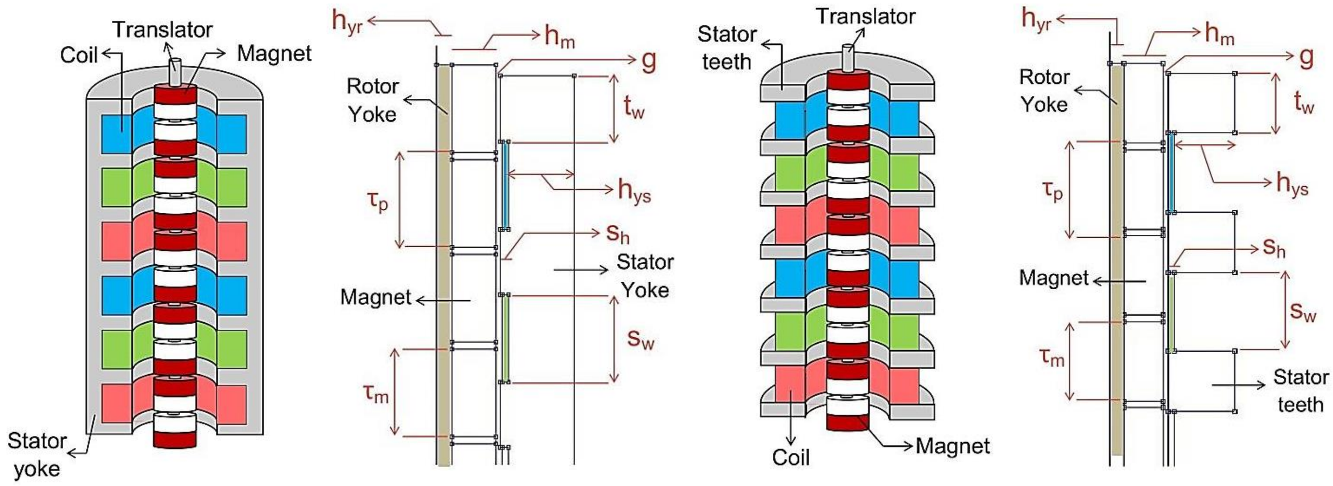

(**a**) (**b**)

Figure 4. Illustration of the two LPMG designs: (**a**) iron-cored; (**b**) semi iron-cored.

Table 1. Dimension of the LPMG designs.

Part, Symbol	Value	Unit
Pole pitch, τ_p	65	mm
Magnet length, τ_m	60	mm
Magnet thickness, h_m	30	mm
Translator yoke thickness, h_{yr}	10	mm
air gap, g	3.5	mm
Tooth width, t_w	45	mm
Slot width, s_w	60	mm
Slot height, s_h	5.5	mm
Stator yoke thickness, h_{ys}	44	mm
Number of the magnet, $2p$	10	units
Translator total length, L_t	645	mm
Number of the slot, n_{sl}	6	units
Stator total length, L_s	630	mm
Number of turn/slot, N_s	220 (iron-cored)	turns
Number of turn/slot, N_s	245 (semi iron-cored)	turns

2.1.2. Semi Iron-Cored LPMG

The semi iron-cored LPMG does not have a complete stator yoke made of ferromagnetic material. In this design (Figure 4b), the stator teeth are still ferromagnetic-based, and thus so are their outward elongations that form a partial stator yoke. However, the spaces between blocks of the elongation teeth (partial yoke) are free-air. Such an arrangement will increase the reluctance of the stator body, reducing the overall flux magnitude and density. To compensate for these decreases, the number of stator windings turns is increased until reaching the same level of the iron-cored flux linkage.

The semi iron-cored LPMG has quite a complicated manufacture (Figure 5). To unite the stator's ferromagnetic bodies, several cylindrical rods are mounted through the edges of each body. The rods are made from non-magnetic material to avoid interaction with the rotor's permanent magnet. Then, nuts and bolts are used to fix the bodies' position on the rod. In this case, the gaps among the bodies are fitted according to the slot width so that the total stator length is nearly equal to the translator length. Meanwhile, to keep the radial position of the yokes and windings, two-cylinder sheets (pipe-shaped) are placed on the inner and outer surfaces of the stator yoke bodies. The sheets are also made of non-magnetic material so that they do not significantly affect the resulted magnetic fields. These additional components and additional winding charge more cost to the semi iron-cored type. However, the iron cost is fewer, as the stator volume is smaller than the iron-cored type. Other cost components including magnets and rotor yoke are equal.

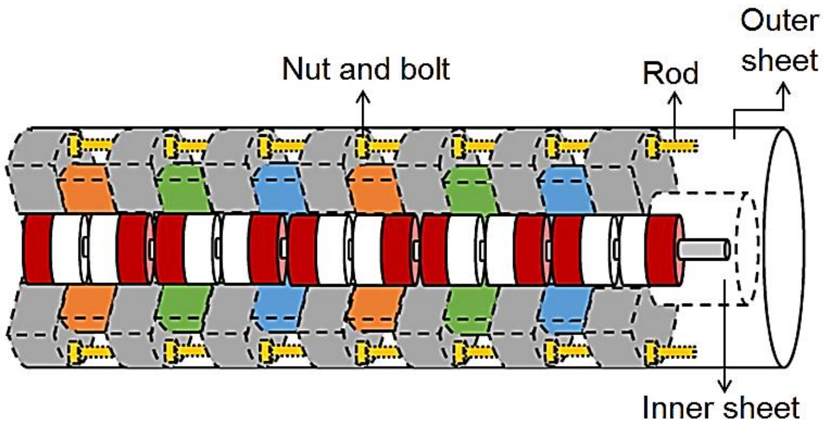

Figure 5. Manufacture illustration of the semi iron-cored LPMG.

Table 1 shows that both LPMG designs have equal overall dimensions since the targeted electrical outputs are also equal. Furthermore, the equal length between the stator and the translator implies that the electromagnetic process that generates electricity will only occur effectively when there is a portion of each component (stator and translator) that face each other. From this design aspect, the effective translator stroke that allows such a condition becomes limited in size yet important as a constraint. In this case, it is equal to the total length of the stator and translator, $L_t + L_w$.

The small-scale designs have also been manufactured to check the validity of the models. The main components are shown in Figure 6. Figure 7 shows the 2D models with the dimensions are tabulated in Table 2. Overall, the dimensions of the real models are roughly one-third of the theoretical dimensions. The stator and translator yokes are made of steel carbon of ST37 with no lamination. The permanent magnets are arranged axially and are made of NdFeB material of N42-type. Furthermore, a cylinder pipe of PVC material is used to help position the iron blocks and the windings. In this case, the pipe also substitutes the air gap function.

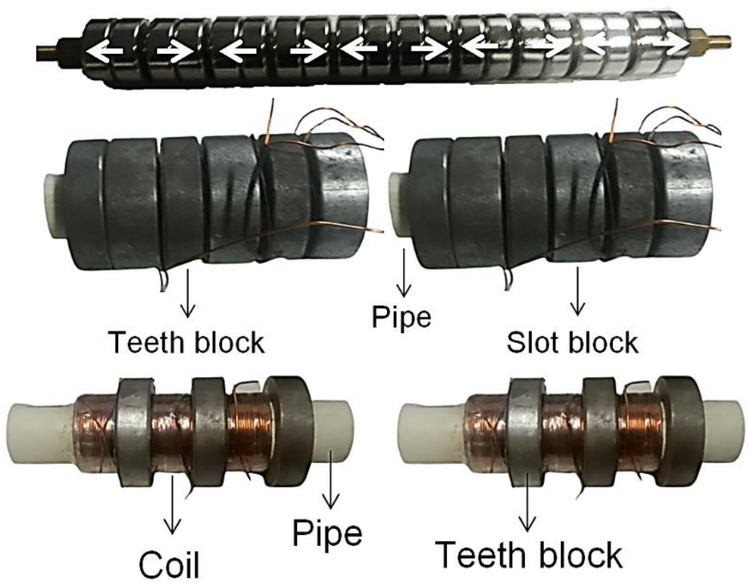

Figure 6. Components of the small-scale LPMG: translator with permanent magnets completed with the magnetic orientations (**top**), iron-cored's stator (**middle**), semi iron-cored's stator (**bottom**).

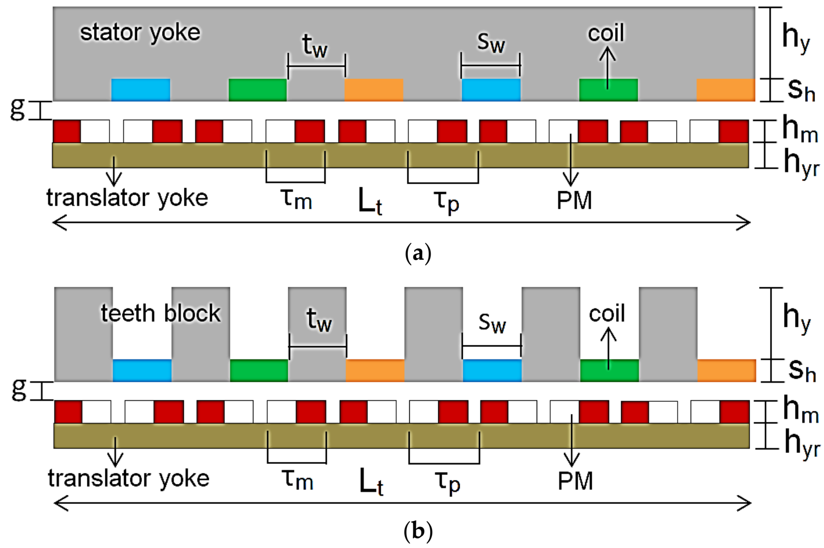

Figure 7. Illustration of the real LPMG design of (**a**) iron-cored and (**b**) semi iron-cored.

Table 2. Dimensions of the real LPMG designs.

Part, Symbol	Iron-Cored	Semi Iron-Cored
Pole pitch, τ_p	22 mm	22 mm
Magnet length, τ_m	20 mm	20 mm
Magnet thickness, h_m	9.5 mm	9.5 mm
Translator yoke thickness, h_{yr}	3 mm	3 mm
air gap, g	3 mm	3 mm
Tooth width, t_w	15 mm	15 mm
Slot width, s_w	20 mm	20 mm
Slot height, s_h	3 mm	3 mm
Stator yoke thickness, h_{ys}	15 mm	15 mm
Number of the magnet, $2p$	10 units	10 units
Translator total length, L_t	218 mm	218 mm
Number of the slot, n_{sl}	6 units	6 units
Stator total length, L_s	210 mm	210 mm

2.2. System Modeling

The modeling of the system's work is presented in Figure 8. In this subsection, the wave build that is used to test the designed LPMGs will be explained first. Then, its motion affects the two main subsystems of the direct-drive WEC: dynamics of the floater and energy conversion in the LPMG. Each subsystem will be detailed later.

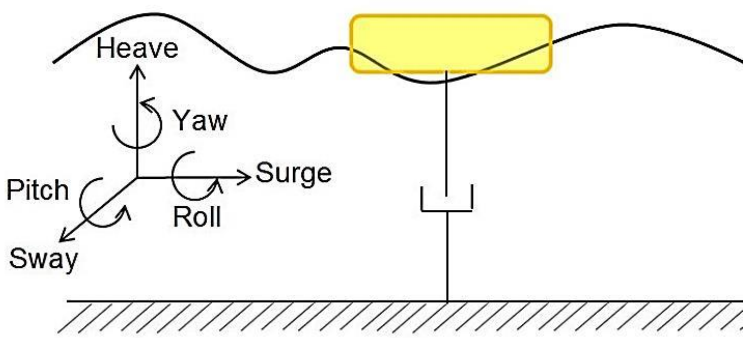

Figure 8. Model of wave motion.

2.2.1. Ocean Wave Samples

Before generating the unidirectional long-crested random waves, some parameters need to be defined: the significant wave height and the peak frequency. In this analysis, wave height data in the southern ocean of Yogyakarta, Indonesia (9°–10°30′ S and 109°10′–111°10′ E) are used. Aside from its potential energy, the location also has at least three advantages in terms of less sedimentation, steep contour, and land texture [47]. As it is the initial designated placement location for both converter types, thus, using the data from this place will measure the effectiveness of the designs themselves but under approaching-real wave situations. The wave height data were extracted using Windwaves-05 numerical modeling [48]. They are presented in form of maps, with the different significant wave heights throughout locations represented by different colors.

Previously, only the average value of the monthly average significant wave height data was used to design the LPMGs [42,43]. However, in this random waves test, the basis data will be expanded to approach the real situation. The absolute highest significant wave heights (one is displayed in Figure 9a) will also be accommodated, not only the monthly average ones (one is shown in Figure 9b). All the data were taken monthly from 2000 to 2010. The use of different significant wave height values is to cover the peak wave condition at the placement location during the tests. Furthermore, they are able not only to test the LPMGs' performances under different circumstances but also to select which wave condition results in maximum output power. Then, the result can be considered in applying similar designs.

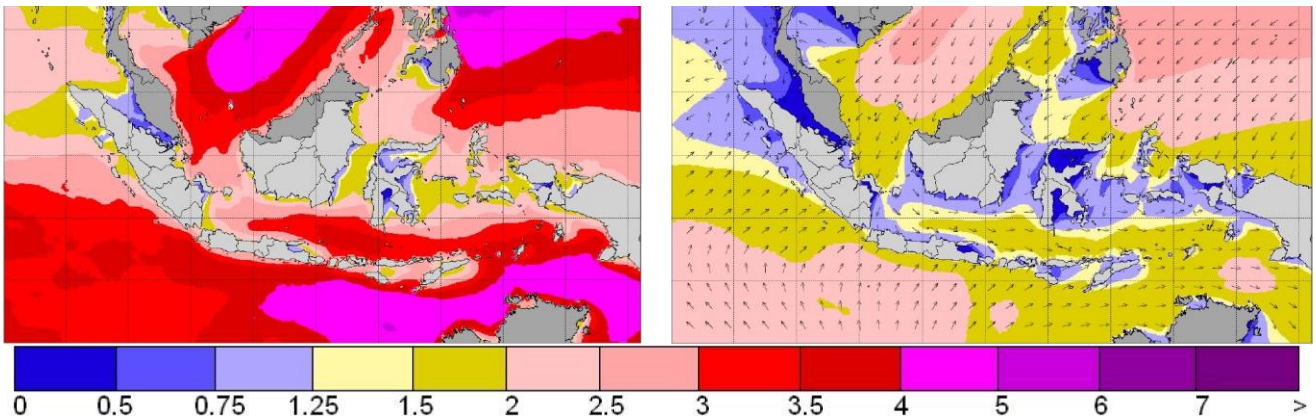

(**a**) (**b**)

Figure 9. Sample of: (**a**) absolute highest significant wave height map; and (**b**) average significant wave height map in January during period of 2000–2010. The color gradation measures the height in meters [48].

The monthly significant wave height data, both average and absolute highest values at the placement location, are shown in Table 3. Several values will be taken as samples to generate the test wave models for the WEC. To relate them with the design aspect, they will be stated as comparisons toward the effective translator stroke, $L_s + L_t$. For equal significant wave height (h_{swh}), the wave peak frequency is varied (Table 4). The variation is resulted from different wave periods, of which several values are picked up. Meanwhile, the wave height is stated at a "moderate" level. On the other hand, the significant wave height is varied as the wave's peak frequency is kept constant (Table 5).

From Tables 4 and 5, all wave parameters' variations have larger significant wave height than the effective translator stroke. This arrangement is useful to measure the design efficiency of the LPMGs. For a certain expected output power, the converter is usually made as small as possible. However, it also has a negative impact, since it results in moments where parts of the stator and translator are not facing each other. The last part will cause an ineffective electromagnetic process that impacts negatively on the electrical output. Then, it is necessary to find out how far the moments influence the output power.

Table 3. Monthly significant wave height data during 2000–2010.

Month	Average Significant Wave Height (m)	Absolute Highest Significant Wave Height (m)
January	1.750	3.500
February	1.750	4.500
March	1.375	3.500
April	1.375	3.000
May	1.750	3.000
June	1.750	3.500
July	2.000	3.500
August	1.500	3.500
September	1.750	3.500
October	1.750	3.000
November	1.750	2.500
December	1.750	3.500

Table 4. Peak frequency variation used in the test.

Period (s)	Peak Frequency (Hz)	Significant Wave Height (m)	$h_{swh}/(L_t+L_s)$	Sea State (Code)
1.2	0.83	2.5 m	1.97	Moderate (4)
1.3	0.77			
1.4	0.71			
1.6	0.61			

Table 5. Significant wave height variation used in the test.

Period (s)	Peak Frequency (Hz)	Significant Wave Height (m)	$h_{swh}/(L_t + L_s)$	Sea State (Code)
1.6	0.61	1.5	1.18	Slight (3)
		2.5	1.97	Moderate (4)
		3.5	2.75	Rough (5)
		4.5	3.53	Very rough (6)

In nature, the ocean waves themselves come in irregular and changeable forms, so determining the exact magnitude of wave's height and frequency is difficult. The values are usually approached by using ocean wave spectral density. This method works by using statistical description, which shows the energy distribution for various wave frequencies. The wave amplitude is commonly referred to as significant wave height, and it lies at the peak frequency. Among several spectral analyses, the Joint North Sea Wave Project (JONSWAP) spectrum has been used in many cases. It is used for fully developed wind-generated waves in open water with no wind blow time range limit [49]. According to this principle, the wave spectrum, $S(\omega)$ is defined in the following equations [50]:

$$S(\omega) = \alpha H^2 \left[\frac{{\omega_i}^4}{\omega^5} \right] exp \left[-1.25 \left(\frac{\omega_i}{\omega} \right)^4 \right] \zeta^{exp[-\frac{(\omega-\omega_i)^2}{2\sigma^2 {\omega_i}^2}]} \tag{2}$$

$$\alpha = \frac{0.0624}{0.23 + 0.0336\zeta - \frac{0.185}{1.9+\zeta}} \tag{3}$$

The above equations include some notations: ω_i is the spectral peak frequency (rad/s), ω is the base frequency (rad/s), H is the significant wave height (m), and σ is the shape parameter constant. Meanwhile, α is Phillip's constant. Notation ζ represents the peakedness parameter (ranging from 1 to 7). Considering Equations (2) and (3), the time series of ocean wave elevation can be generated by using the following equations

$$\eta(x, y, t) = \sum_{i=0}^{N} a_i sin(\omega_i t + \beta_i - k_i x cos\gamma - k_i y sin\gamma) \tag{4}$$

$$\alpha_i = \sqrt{2S(\omega_i)\Delta\omega} \tag{5}$$

Equations (4) and (5) reflect that a random wave η at a location (x,y) can be defined as a sum of i^{th} regular or harmonic waves (m) in which the amplitudes of the individual wave component is a (m), propagating at angle γ with respect to the initial coordinate frame, wave number of k_i (rad/m), and a random phase β_i (rad) with uniform distribution produced in the range of $[-\pi, \pi]$. Meanwhile, $\Delta\omega$ indicates the wave frequency resolution. Given the ocean depth of d_w (m), wave period of *T(s)*, and gravitational acceleration of g (m/s^2), the wave length can be calculated using Equation (6) via the iteration method, and the corresponding individual wave number k can be calculated accordingly.

$$\lambda_i = \frac{gT^2}{2\pi} tanh\left(\frac{2\pi d_w}{\lambda_i}\right); k_i = \frac{2\pi}{\lambda_i} \tag{6}$$

By assuming that the ocean water is irrotational, incompressible, having a flat base, and having the mass conserved, the instantaneous water particle velocity and acceleration in the x–y axes can be computed by the equations below [51]

$$u(t) = \omega \frac{cosh(ks)}{sinh(kd)} \eta(t);\ w(t) = \omega \frac{sinh(ks)}{sinh(kd)} \dot{\eta}(t) \tag{7}$$

$$\dot{u}(t) = \omega \frac{\cosh(ks)}{\sinh(kd)} \dot{\eta}(t);\ \dot{w}(t) = \frac{\sinh(ks)}{\sinh(kd)} \ddot{\eta}(t) \tag{8}$$

Notation u and w as well as their derivatives represent the particle's velocity and acceleration along the x-axis and y-axis, respectively. Variable s is the distance of the instantaneous center of the floater from the seabed (m). θ is wave phase (m), as in Equation (4).

2.2.2. Dynamic Modeling of the Floater

Under the impacts of ocean waves in the xyz coordinates, the floater undergoes six-coupled motions (Figure 8), which are defined as surge: displacement along x-axis, heave: displacement along y-axis, sway: displacement along z-axis, roll: rotation about x-axis, yaw: rotation about y-axis, and pitch: rotation about z-axis [52]. The wave motions will determine the floater position and displacement; thus, they will affect the slider and the translator movement. When the floater is submerged into open water and a random wave propagates through it, it will experience fluid loading and will oscillate. Since it is connected to the converter through a slider, the wave mechanical energy is transferred to the converter via the slider. The dynamics of the floater is expressed by the below equations [53]

$$(m + M_\infty)\ddot{y}(t) + \int_0^t K(t - t')\dot{y}(t')dt' + Gy(t) = F_e(t) + F_{PTO}(t) \tag{9}$$

$$F_{PTO}(t) = -B_{PTO}\dot{y}(t) \tag{10}$$

Notations in above equations: m is the cylinder mass (kg), M_∞ is the added mass at an infinite frequency (kg), $\ddot{y}$ is the vertical acceleration of the cylinder (m/s^2), $\dot{y}$ is the vertical velocity of the cylinder (m/s), K is the impulse response function (IRF), t is time (s), B_{PTO} is the power take-off damping coefficient, G is the hydrostatic stiffness, *y(t)* is the vertical position of the cylinder (m), and F_e is the excitation force (N). In this paper, IRF in Equations (9) and (10) are solved using the Marine Systems Simulator (MSS) toolbox developed by Thor I. Fossen's team at Norwegian University of Science and Technology [54]. Once all the parameters are obtained, the dynamic responses are computed via MATLAB Simulink. The results become input for the design of LPMG as discussed in the next subsection.

2.2.3. The Work of the LPMG Converter

The dynamics of the translator (based on random wave's work on the floater) affect the magnetic field on the stator coils. The magnetic flux flows from the magnets to the stator teeth and yoke. As a result of the translator movement, the flux magnitude fluctuates. As a result, electromotive forces (emf) are induced on the coil terminals. First, the flux distribution is simulated using FEMM software. The flux magnitude per magnet is [55]

$$\varnothing_{PM,pk} = 2B_{m,pk}\pi\left(h_{yr} + h_m\right)\tau_p \tag{11}$$

$\phi_{PM,pk}$ is the peak flux magnitude resulted from a magnet (Wb), and $B_{m,pk}$ is the peak permanent magnet flux density (T). The flux flows are shown in Figure 10. The flux magnitude for each winding phase can be calculated using the below formula [56]

$$\varnothing_{p,pk} = 2B_{g,pk}\pi\left(h_{yr} + h_m + g\right)\tau_p k_w \tag{12}$$

$\phi_{p,pk}$ is the peak flux magnitude in each phase (Wb), $B_{g,pk}$ is the peak air gap flux density (T), and k_w is the winding coefficient. After gaining the flux linkage per phase, the electrical output can be calculated analytically. The induced voltage in each phase is [57,58]

$$e(t) = N_{ph}\frac{d\varnothing(t)}{dt} = N_{ph}\frac{d\varnothing(t)}{ds(t)}\frac{ds(t)}{dt} \tag{13}$$

e(t) is the momentary induced voltage or electromotive force (V). The term *ds(t)/dt* represents the instantaneous speed (m/s) at a certain translator position of *s(t)*.

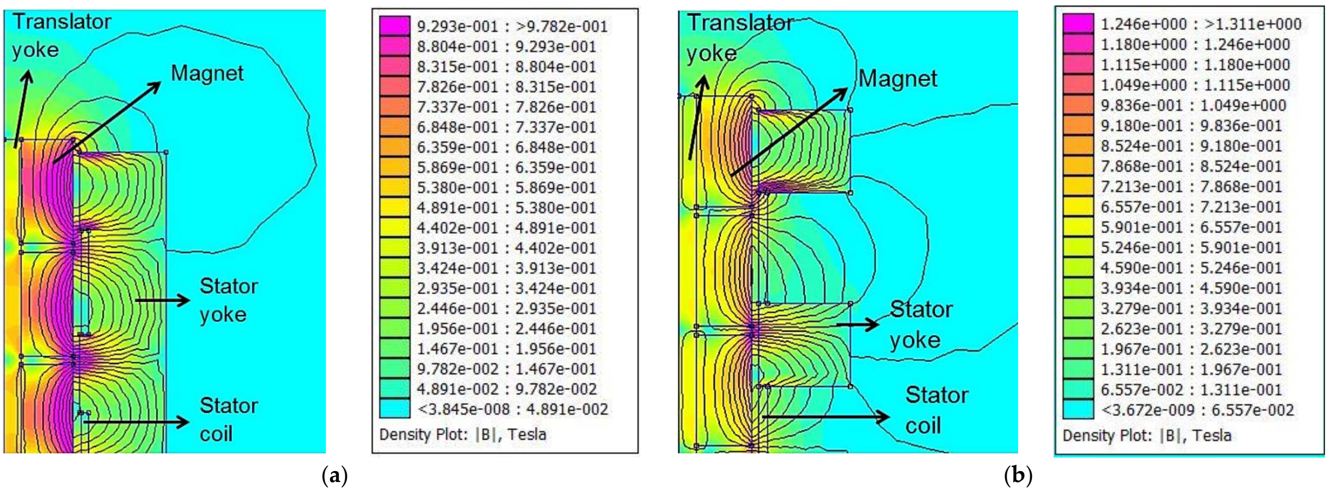

Figure 10. Absolute magnetic flux density (|B|) in (**a**) iron-cored LPMG and (**b**) semi iron-cored LPMG.

Under load conditions, the active output power of the generator is directly proportional to the induced voltage but is inversely proportional to the coil impedance. The coil impedance is composed of the coil's reactance and inductance, whose values depend on the winding configuration. Assuming that the load is a pure resistance, then

$$Z_\theta = \sqrt{\left(R_s{}^2 + R_L{}^2\right)} + X_s \tag{14}$$

$$X_s = 2\pi f(L_s + L_m) \tag{15}$$

$$L_s = \frac{d\varnothing_a}{di_a}; L_m = \frac{d\varnothing_a}{di_b} \tag{16}$$

Notation Z_θ is phase impedance (Ω); R_s and R_L are line resistance and load resistance, respectively (Ω). X_s is line reactance (Ω), while L_s and L_m are self and mutual inductances of the winding (H). ϕ is coil flux linkage (Wb) and i is the phase current (A), while their subscripts' letters represent the same or different phase.

Then, the terminal voltage and the output power of the LMPG are

$$V_T = e - i_L(R_s + X_s); i_L = \frac{e}{Z_\theta} \quad (17)$$

$$P_o = \sum V_T i_L \quad (18)$$

i_L represents the load current (A), V_T is terminal voltage (V), and P_o is output power (W). The sigma operation in Equation (18) shows the cumulative calculation from all phases.

On the other hand, both LPMGs also dissipate losses. There are three main electrical loss components. The copper loss (P_{cu}, in watt) results when the load current flows on the coils. The wire's copper has a certain value of resistance that dissipates loss.

$$P_{cu} = \sum {i_L}^2 R_s \quad (19)$$

Meanwhile, the core loss is suffered in the translator and stator core. There are two main components of the loss: hysteresis loss (P_H) and eddy current loss (P_E); both are stated in watts.

$$P_h = k_H f {B_m}^{1.6}(V_s + V_r) \quad (20)$$

$$P_E = \frac{\pi^2 f^2 {B_m}^2 {t_l}^2 (V_s + V_r)}{6\rho_r} \quad (21)$$

k_H is the hysteresis coefficient, while V_s and V_r are stator and translator yoke volume (m^3), respectively. B_m represents the maximum stator flux density (T), t_l is lamination thickness (m) of the core, f is the frequency (Hz), and ρ_r is the core resistivity (Ω/m).

$$V_s = n_{sl}\pi\left\{t_w\left[\left(h_{yr} + h_m + g + s_h + h_{ys}\right)^2 - \left(h_{yr} + h_m + g\right)^2\right] + s_w\left[\left(h_{yr} + h_m + g + s_h + h_{ys}\right)^2 - \left(h_{yr} + h_m + g + s_h\right)^2\right]\right\} \quad (22)$$

$$V_r = \pi {h_{yr}}^2 L_t \quad (23)$$

Equation (22) is for the iron-cored type. For the semi iron-cored type, the second term inside the curly bracket is eliminated; thus, the value will be smaller. Finally, the electrical efficiency (η, in %) of the LPMG can be calculated from the output power and the resulted power loss.

$$\eta = P_o/(P_o + P_{cu} + P_H + P_E)100 \quad (24)$$

The output power profile of a WEC can be approached from the input wave, since the translator's movements depend on the wave's work on the floater. However, in a unidirectional long-crested random wave scenario, the wave elevations do not follow a certain polynomial function. An incoming wavefront is a combination of different single regular waves with different amplitudes that continuously changes during the iteration process. Therefore, the wave amplitude will vary throughout time. In this case, the changes of the wave amplitude are significant in the electromagnetic process considering the shorter effective translator stroke. The last parameter itself affects the electromagnetic process in certain positions, so the influence of each factor needs to be clearly defined.

3. Results and Discussion

In this section, the unidirectional long-crested random waves, the floater dynamics based on the random waves, and the electrical output of the LPMGs will be explained.

3.1. Resulted Random Waves

From the selected values of significant wave height and peak frequency, first, the JONSWAP energy spectrums are calculated. They are shown in Figure 11. The energy spectrums for equal frequency random waves are directly proportional to the significant wave height values. Meanwhile, the peak frequency is equal among all wave height values;

hence, the peak energy spectrums lie at the same frequency. On the other hand, for the equal significant wave height, the peak energy spectrum is inversely proportional to the peak frequency. In this condition, the lower peak frequency random waves will bring a larger amount of energy than the higher peak frequency ones.

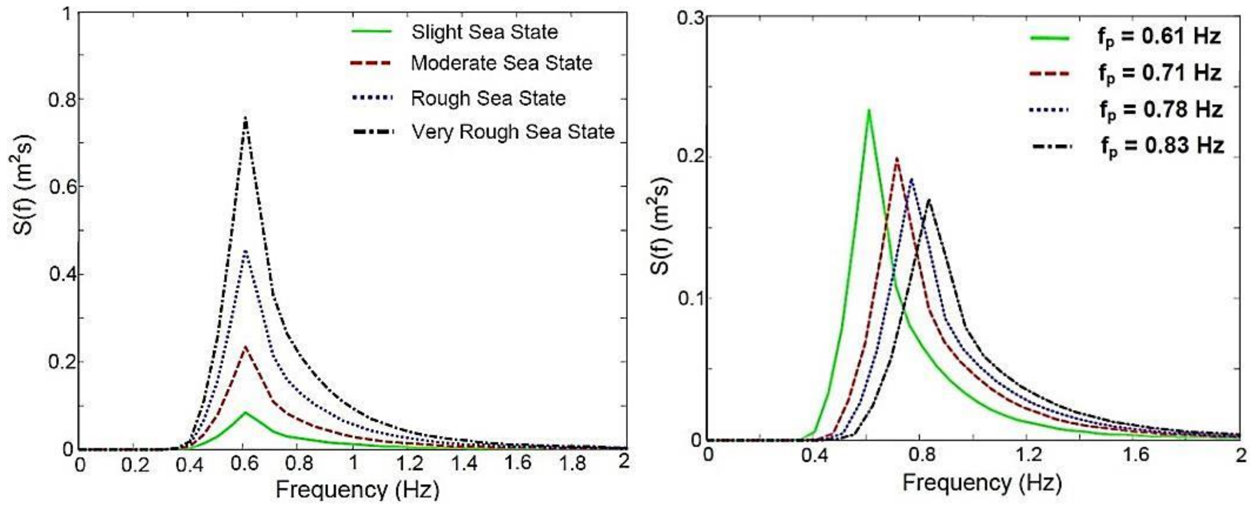

Figure 11. JONSWAP energy spectrum unidirectional long-crested random waves with different: significant wave height (**left**); peak frequency (**right**).

After defining the energy spectrum, the wave's particle elevations are calculated. It will be used to plot the floater's vertical deviations under the respective random waves. The change in floater position will result in the translator movement, which will generate electricity (Equation (13)). The plotting is conducted for 999.9 s with 0.1 s intervals. The resulted wave elevation is directly proportional to the basic significant wave height, as the overall wave height and the maximum height among the waves are proportional to it (Figure 12). Meanwhile, different peak frequencies overall result in relatively similar wave height (Figure 13). After obtaining the wave elevations from all wave parameters' variations, the positions of the WEC's floater can be extracted.

3.2. Floater Dynamics under Random Waves

The wave motions will move the floater and translator in synchronized motions. Figure 14 shows the resulted floater deviations under random wave configurations compared to those under the initial sinusoidal wave for several sampling times. The different wave characteristics result in different floater moving patterns in certain periods. Some points are explaining the resulted vertical deviations from different random wave parameters.

First, the floater deviation is proportional to the wave elevations, which are linear to the significant wave height. Figure 14(left) shows that the random wave with higher significant wave height results in a higher floater's vertical deviation. Meanwhile, in Figure 14(right), different peak frequency random waves result in similar deviation, as the resulted wave's particle elevations are also similar to each other (Figure 13). Next, the deviation changes will determine the instantaneous vertical speed (Figure 15). In this case, the relation between the deviation and speed results in the derivation of the wave parameters trends as shown in Figure 14. Then, the significant wave height is linearly proportional to the average vertical speed. Inversely, as the peak frequency decreases, the average vertical speed slightly increases. Table 6 tabulates the floater's deviation and speed under different significant wave heights and peak frequencies.

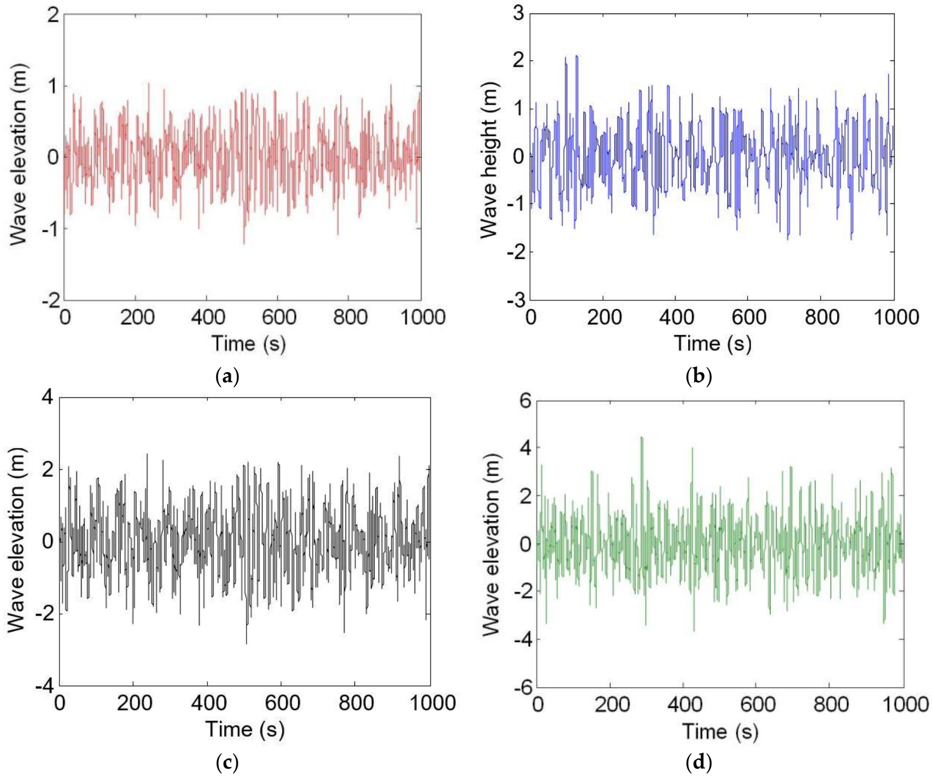

Figure 12. Wave elevation graphs for random waves with equal peak frequency and significant wave height values of (**a**) 1.5 m; (**b**) 2.5 m; (**c**) 3.5 m; (**d**); 4.5 m.

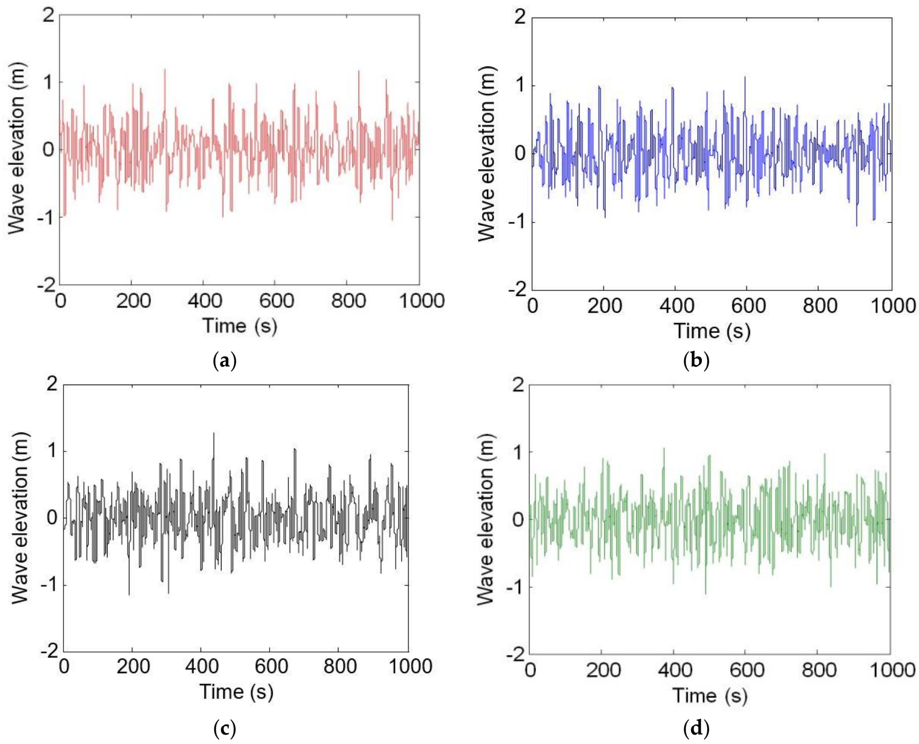

Figure 13. Wave elevation graphs for random waves with equal significant wave height and peak frequency values of (**a**) 0.83 Hz; (**b**) 0.77 Hz; (**c**) 0.71 Hz; (**d**) 0.61 Hz.

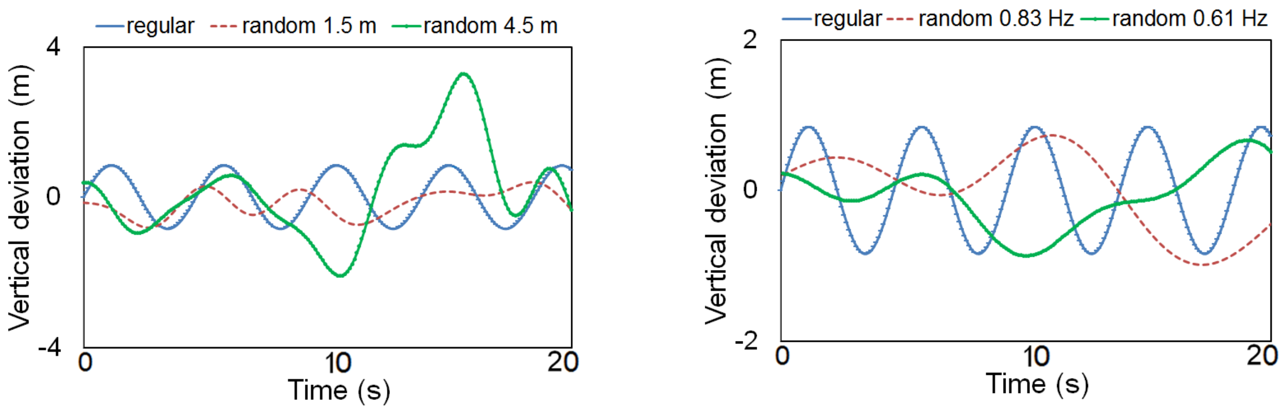

Figure 14. Floater vertical deviations resulted from a regular wave compared to random waves with different significant wave height-equal peak frequency (**left**), and to random waves with different peak frequency-equal significant wave height (**right**).

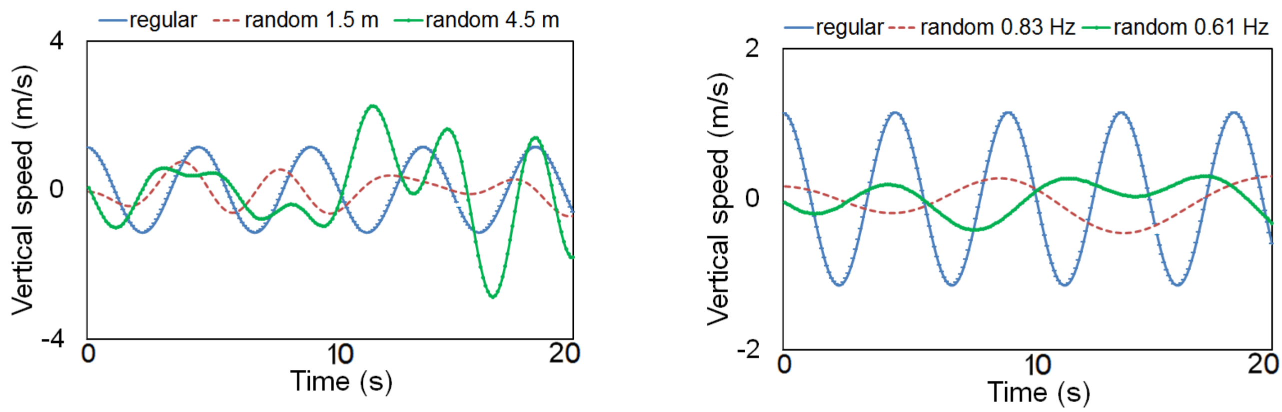

Figure 15. Floater vertical speeds resulted from a regular wave compared to random waves with different significant wave height-equal peak frequency (**left**) and to random waves with different peak frequency-equal significant wave height (**right**).

Table 6. Average floater's vertical deviation and vertical speed from different random waves.

Peak Frequency (Hz)	$h_{swh}/(L_t + L_s)$	Average Vertical Deviation (m)	Average Vertical Speed (m/s)
0.83	1.97	0.291235	0.157415
0.77		0.282691	0.161938
0.71		0.288943	0.165331
0.61		0.298978	0.179483
0.61	1.18	0.306962	0.275330
	1.97	0.519600	0.284100
	2.75	0.716133	0.642433
	3.53	0.893543	0.886968

For random waves with a significant wave height of higher than 2.5 m, the average floater deviations are higher than that from the initial regular wave. However, only a wave with a significant wave height of 4.5 m results in a higher average vertical speed than the regular wave. The wave mechanisms under regular scenarios are running stably and continuously, while in unidirectional long-crested random waves, the instantaneous values fluctuate irregularly. Then, that different trend results in a diverse average value. Meanwhile, the average floater's deviations and vertical speed from all peak frequencies are smaller compared to that from the initial wave.

The vertical speed is proportional to the translation speed, which will govern the electromotive force. In an equal translator-stator position, higher instantaneous vertical speed will result in higher momentary induced voltage. From the data in Table 6, it is reasonable to approximate that the electrical output of the WEC under the random waves will be smaller than that from the regular one, unless for a significant wave height of 4.5 m.

However, there is another effect that also plays a significant role. The average vertical deviation represents half of the average floater amplitude. The amplitude itself is linear to the displacement covered by the translator when moving between its two farthest ends. Compared to the effective translator stroke, random waves with a significant wave height of more than 2.5 m result in higher amplitudes. Nevertheless, all different wave parameters also have moments where the instantaneous floater amplitudes are higher than the effective stroke. This is because all wave variations have a larger significant wave height setting. Since the moments negatively affect the output voltage and power, there will be mixed influences along with the vertical speed factor.

3.3. Output of the LPMG

First, Figure 16 (left) shows the induced voltage from both LPMGs under no wave influence. The translation speed is set constant at 1 m/s. Since the semi iron-cored LPMG has undergone modification in the number of turns (to compensate for the incomplete iron body), its resulted voltages are similar to the iron-cored. The constant unity speed put aside the *ds(t)/dt* component, meaning this is the 'basic' induced voltage graph of both LPMG designs, regardless of the wave mechanisms that drive it. In this case, the translator moves uniformly from one end to another. The voltage first rises gradually until reaching the peak and then decreases. The maximum value is achieved at the optimum position: when the translator is directly facing the stator in a parallel position.

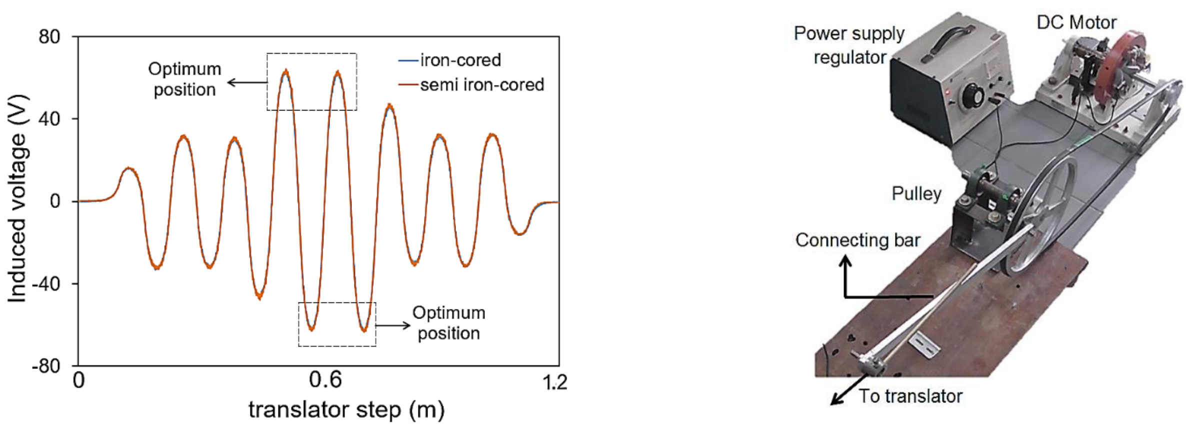

Figure 16. The induced voltage of the LPMGs under 1 m/s speed (**left**) and experiment setup with small-scale models (**right**).

An experiment has been performed to measure the real output of the mini-models of LPMGs. The setup is shown in Figure 16 (right). A belt is connecting a DC motor and a pulley. At the edge of the pulley, a metal bar is installed, which is connected to the translator. When energized, the DC motor will rotate the pulley through the belt. Next, the metal bar converts the rotating motion into linear motion, which will be delivered to the translator. In this experiment, the translation speed is 1 m/s. It can be set by regulating the DC motor speed, considering the ratio of the motor's axis diameter and the pulley diameter.

Figure 17a,b show the output voltage of the small-scale models compared to the theoretical output from simulation and analytical calculation. Overall, the resulted sinusoidal graphs agree with the analytical calculation, with the resulted voltage from both real models being about one-seventh of the theoretical value. Then, it is assumed that the trends will also be relatively close in unidirectional random wave conditions.

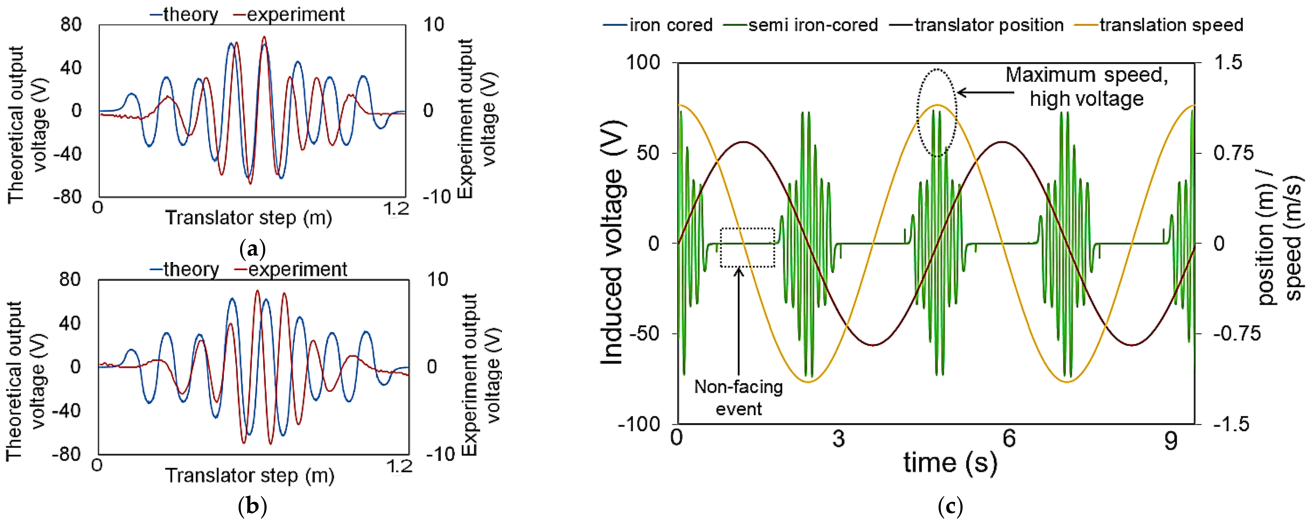

Figure 17. The graphs of the induced voltage of (**a**) iron-cored LPMG and (**b**) semi iron-cored LPMG from calculation and experiment; (**c**) induced voltage of LPMG designs under the regular wave.

Figure 17c presents the LPMGs' operations under regular wave conditions. The shorter stator and translator lengths compared to the applied wave amplitude cause several disjoints in the voltage graph. The disjoints reduce the effective output voltage and power. However, the LPMG can still produce the expected power, because the LPMG establishment is arranged to gain the highest translation speeds in the optimum position. In a regular scenario, this arrangement is easier to conduct since the wave dynamics are mathematically simpler to model. The high speed that drives the translator when it directly faces the stator (optimum position) will result in high voltage and high output power. In Figure 17c, the maximum voltage is resulted at the maximum speed. Then, the maximum voltage and power compensate for the disjointed outputs. From a design aspect, it allows the LPMGs' sizes to be fitted and compacted.

On the other hand, the induced voltages under random wave variations are shown in Figures 18 and 19. In random wave conditions, both the position and the translation speed (proportional to the floater's vertical speed) mechanisms do not refer to any regular pattern (Figures 14 and 15). Their values depend on the momentary excitation force of the wave. The maximum speed or high speeds do not always occur during the optimum position. The term of optimum position means the position where the translator vertical deviation (y-axis) equals zero (Figure 20(left)). Consequently, the higher speed that drives the translator in not optimum positions may result in lower voltage than the lower speed that occurs during the optimum position. Thus, even though the translation speed is proportional to the resulted voltage, under random waves, it still depends on the translator-stator's instantaneous position. In Figures 18 and 19, the maximum voltage does not always result in the maximum translation speed.

Parts of the not optimum position refer to the non-facing event (Figure 20(right)). When the effective translator stroke is shorter than the floater amplitudes, there are moments when the floater movements position the translator not facing the stator completely. In this position, the leakage flux rises and the flux flows to the stator drops (Figure 20(right)), thus reducing the induced voltage significantly. Then, the frequency of the event is inversely proportional to the overall induced voltage.

From a design aspect point of view, the LPMG needs to be installed with a longer translator to avoid the event. However, it will make a significant increase in manufacturing cost and total weight (additional magnet and translator yoke). Figure 21 presents the percentage of time spent by the facing and non-facing events under the unidirectional long-crested random wave conditions. The higher the significant wave height, the higher the total duration of the non-facing event. Meanwhile, the peak frequency variation results in a similar percentage.

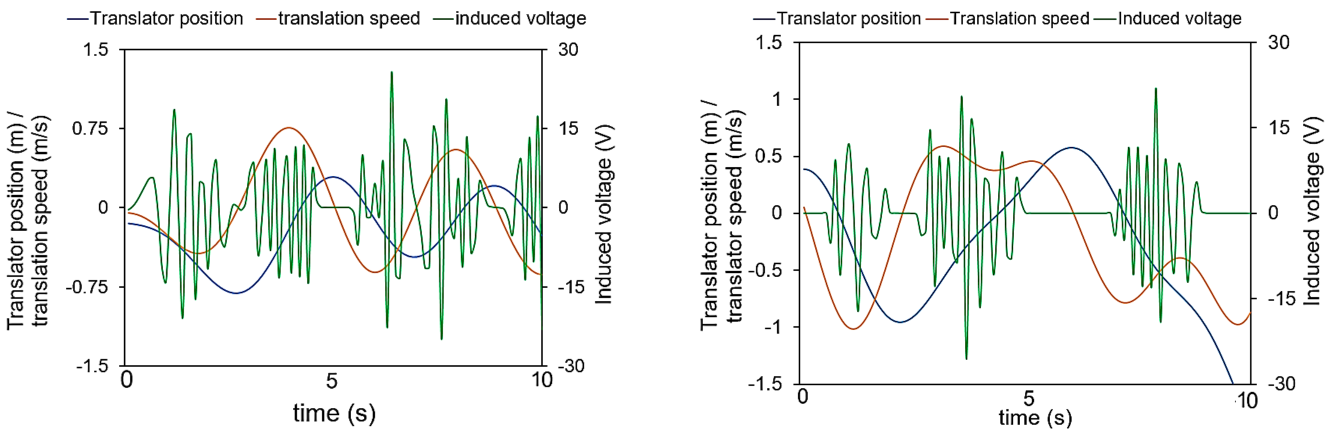

Figure 18. The graph of the induced voltage of the iron-cored LPMG under random wave with equal peak frequency, different significant wave heights of 1.5 m (**left**) and 4.5 m (**right**).

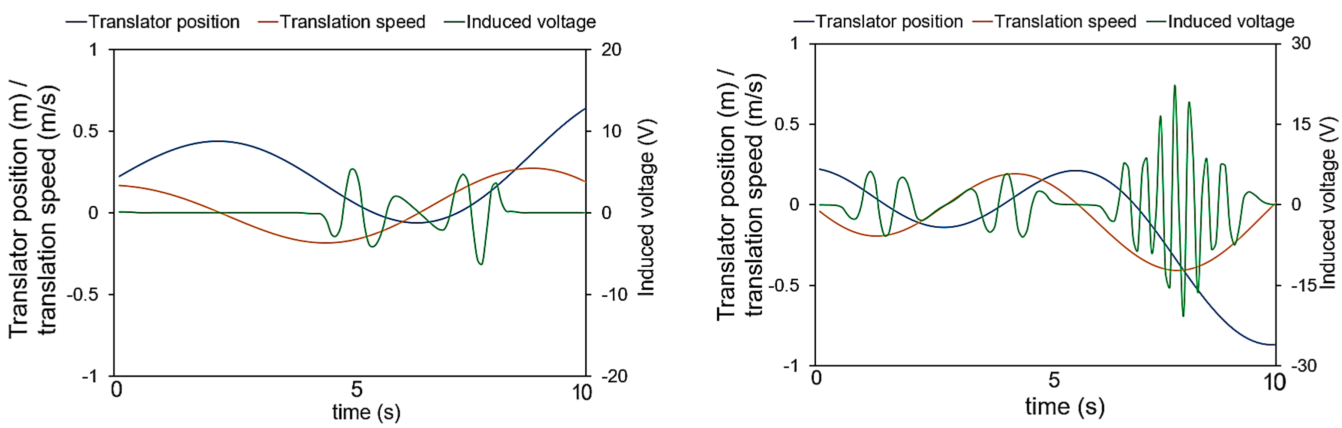

Figure 19. The graph of the induced voltage of the semi iron-cored LPMG under random wave with equal significant wave height, different peak frequencies of 0.83 Hz (**left**) and 0.61 Hz (**right**).

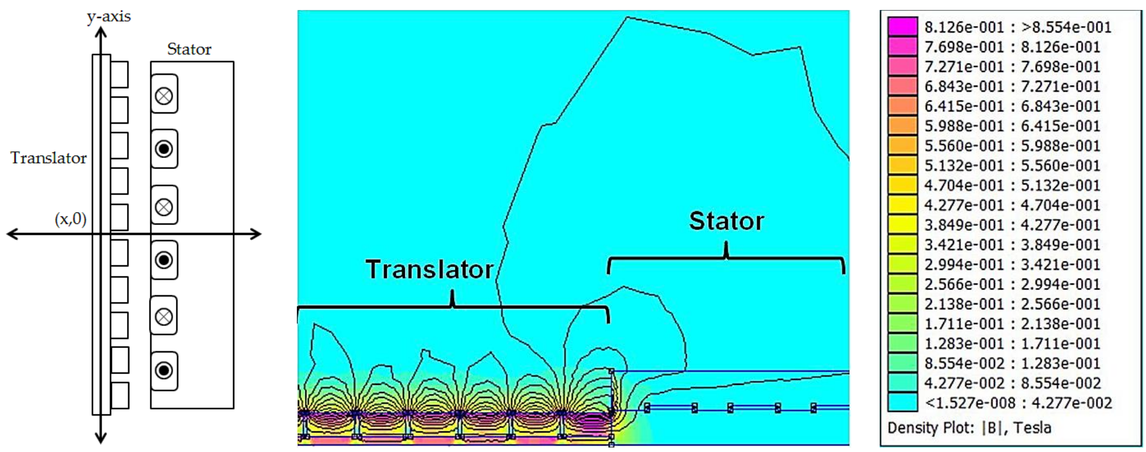

Figure 20. Optimum position (**left**) and flux density (B) in the non-facing event (**right**).

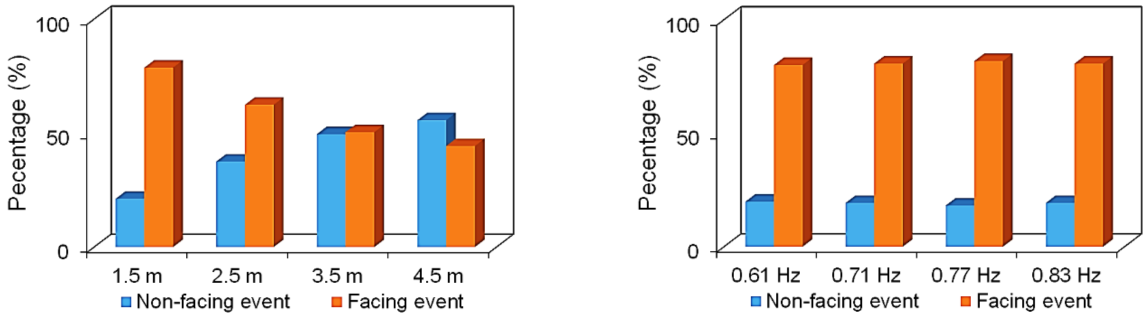

Figure 21. The duration percentages of the non-facing event and the facing event under a random wave with different significant wave height (**left**) and peak frequency (**right**).

Then, from the induced voltage, the output power can be calculated. Figure 22 shows the output power graphs from both LPMG designs under different random wave configurations. They make irregular forms with several disjoints (where the output values are close to zero) due to the non-facing events. Previously, the disjointed graphs were also resulted under regular wave tests [44]. The design process under sinusoidal wave assumption allowed the translator length to be shorter than the wave amplitude, thus causing the events. In the next explanations, the output power will be analyzed in two aspects: maximum and effective (root mean square) values. The first is a measure of the system's ability to produce as maximum output power as possible. Meanwhile, the latter value is used to analyze the overall delivered output power considering the limited and fixed dimension of the LPMG as well as the irregular wave forms.

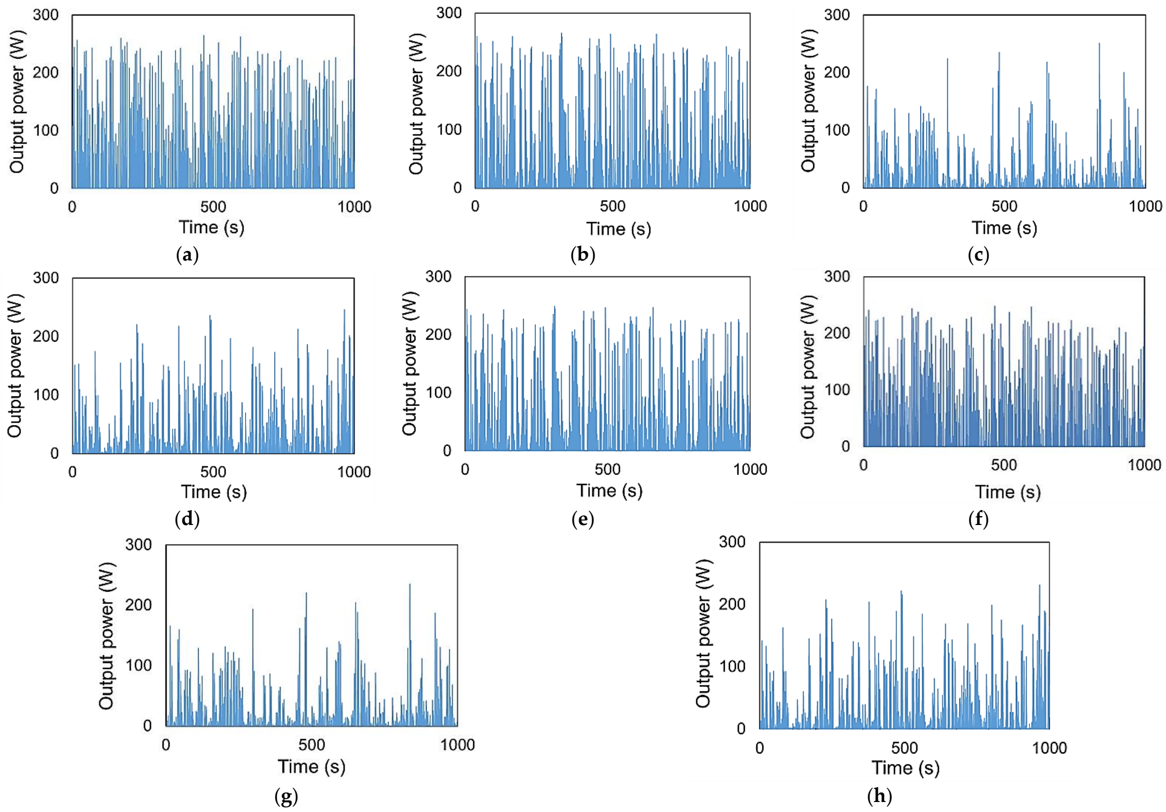

Figure 22. Output power graphs of iron-cored LPMG under random wave with (**a**) 1.5 m significant wave height; (**b**) 4.5 m significant wave height; (**c**) 0.83 Hz peak frequency; (**d**) 0.61 Hz peak frequency, and of semi iron-cored LPMG under random wave with (**e**) 1.5 m significant wave height; (**f**) 4.5 m significant wave height; (**g**) 0.83 Hz peak frequency; (**h**) 0.61 Hz peak frequency.

Figures 23 and 24 show the effective and maximum output powers of both LPMGs under different wave variations for various load resistances. Then, the values for all configurations are tabulated in Table 7. In previous induced voltage in random waves' discussion, the resulted voltage is affected by two factors: the instantaneous translation speed that moves the translator and the translator position itself. Therefore, the output power under different wave parameters can be analyzed from two parameters: the floater's average vertical speed and the non-facing frequency.

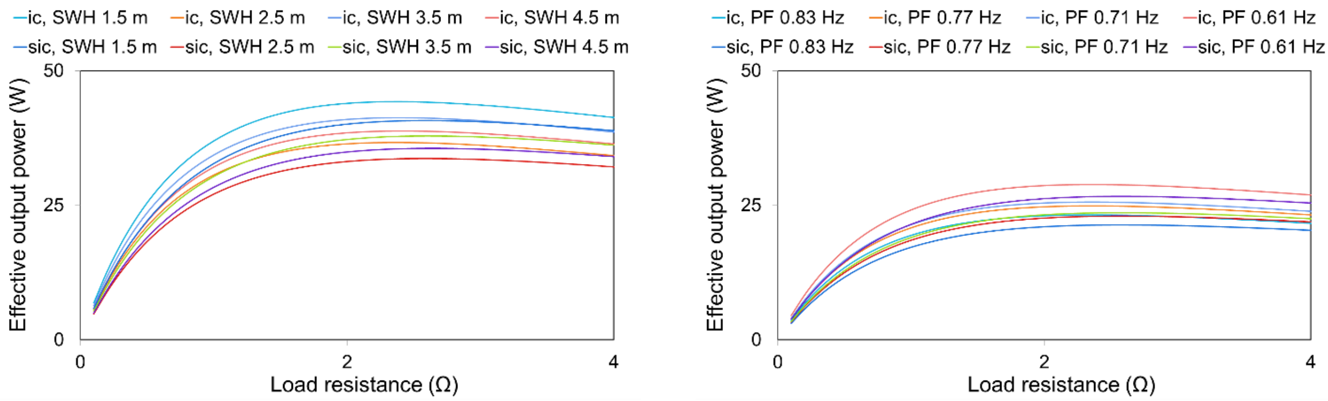

Figure 23. Effective output power resulted from different LPMG designs under different random wave parameters and load resistances (ic: iron-cored, sic: semi iron-cored, SWH: significant wave height, PF: peak frequency).

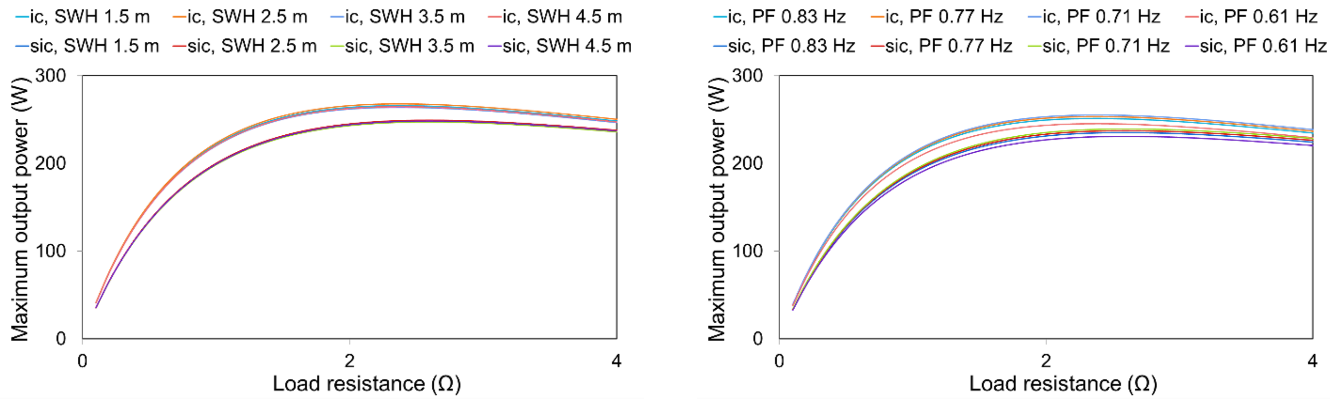

Figure 24. Maximum output power resulted from different LPMG designs under different random wave parameters and load resistances (ic: iron-cored, sic: semi iron-cored, SWH: significant wave height, PF: peak frequency).

Table 7. The effective and maximum output power of the LPMG designs under random wave variations.

Peak Frequency (Hz)	$h_{swh}/(L_t + L_s)$	With Non-Facing Event				Without Non-Facing Event			
		Effective Power (W)		Maximum Power (W)		Effective Power (W)		Maximum Power (W)	
		IC	SIC	IC	SIC	IC	SIC	IC	SIC
0.83	1.97	23.19	21.34	251.22	235.13	25.83	23.77	251.22	235.13
0.77		24.87	22.98	253.35	237.25	27.50	25.40	253.35	237.25
0.71		25.58	23.60	255.17	239.30	28.48	26.27	255.17	239.30
0.61		28.85	26.65	245.34	230.88	32.23	29.78	245.34	230.88
0.61	1.18	44.24	40.74	265.77	249.08	49.85	45.90	265.77	249.08
	1.97	36.66	33.68	267.82	249.21	46.39	42.62	267.82	249.21
	2.75	41.26	37.87	263.87	247.26	58.10	53.33	263.87	247.26
	3.53	38.80	35.57	264.65	248.29	58.29	53.43	264.65	248.29

For both designs, the output powers under different significant wave heights have no specific trend. It is due to the mixed effect as mentioned in the previous subsection. While the average vertical speed that drives the translator is linear to the significant wave height, the frequency of the non-facing event also increases as the wave height rises. The first and second factors successively contribute in positive and negative ways to the output voltage and power. Then, the combination of the driving wave's effects results in no specific trend in the output power.

On the other hand, the peak frequency is inversely proportional to the output power. This is in accordance with the JONSWAP energy spectrum as well as the average floater vertical speed trends. The higher vertical speed is linearly proportional to the induced voltage. Under an equal load, the output power is also proportional to the voltage. Meanwhile, the non-facing event frequency is relatively the same among different peak frequency random waves; thus, it has a similar influence on the output power trend.

Meanwhile, the output powers of the iron-cored LPMG are higher than the semi iron-cored ones. The comparison applies to equal random wave configurations. This is because the semi iron-cored has more winding than the iron-cored; hence, more impedance is formed. For similar induced voltage between the two LPMGs, the higher impedance will decrease the load current and the terminal voltage, which are two components composing the output power. The relation also applies to all load resistances. Figures 23 and 24 also show the output powers trend for several load values. The output power of both designs initially rises as the load is increased. After reaching the peak, the output power slightly decreases to a convergent state.

Regarding the output powers resulting from different significant wave heights compared to those from peak frequency variation, there are two influencing factors. From Table 6, the significant wave height variation produces a higher average vertical speed than the different peak frequencies. The vertical speed that next produces translation speed is linearly proportional to the induced voltage (Equation (13)) and linear to the output power (Equations (17) and (18)). On the other hand, the different significant wave heights also result in more frequent non-facing events than the peak frequency variation. Consequently, some of the high translation speeds occur during the moment. In case it happens, the higher translation speed will not positively affect the output voltage and the output power. Comparing the output powers resulting from both wave parameters' variation, the higher translation speed's effect outweighs the effect of the non-facing event.

There are also differences between the output powers from both designs compared to the rating of the LPMGs. This shows that under the unidirectional long-crested random wave, the designs (with their dimensions) have not been able to fulfill the expected output. Here, two notable factors can be considered in improving the LPMG designs. First, the wave height data in the placement location show the presence of high wave amplitudes in some periods. To model the wave as realistically as possible, those data are included in the random waves' formation. Then, it causes a significant difference between the wave amplitude and the effective translator stroke. As a result of the event, the output power drops in some moments. Second, the LPMG design should also be considered. Under the unidirectional long-crested random wave scenario, the wave elevation and speed fluctuate irregularly throughout time. To optimize the output power, the shorter and limited dimension of the stator and translator should be able to gain high translation speeds during optimum position.

To understand the significance of the non-facing events to the output power, the outputs from the events need to be eliminated. In Table 7, the output powers without the non-facing event are also presented. For both designs, the effective output powers are increasing. The changes show the negative impact resulted from non-facing events. The nearly zero output power during the events decreases the overall output. Meanwhile, the maximum powers are the same because they resulted during the facing event; thus, eliminating the non-facing event produces no effect. For different peak frequencies, the increase of the effective power is similar, because the non-facing event duration is similar between different frequencies. The increase is also not significant, as the non-facing event spends a minority time portion compared to the facing event. Meanwhile, the non-facing event frequency is linear with the significant wave height. Thus, the increase of the output power is rising with the increase of the height.

However, the increase in the effective output power is not significant enough to reach the expected output. The maximum output powers are also below the expected value. In this case, the more influencing factor is the LPMGs' inability to harness high translation speeds within its effective translator stroke range. Unlike the regular wave, the dynamics of the unidirectional long-crested random wave do not follow any regular pattern. Thus, for LPMGs whose dimensions are shorter than the wave amplitude, not only are they vulnerable to the non-facing event, it is also difficult to position them or to arrange the translator-stator relative position so that it can optimally harness the wave's high vertical speeds. Under regular waves, the LPMGs still experience non-facing events but are still able to produce the expected output.

Thus, in designing the LPMG-driven WEC, the shorter translator (than the wave amplitude) model cannot be employed. The easier way to improve is by extending the dimension, approaching or even equalizing the wave amplitude at the placement site. However, it still needs to be investigated whether other components also require upgrading. Furthermore, design optimization is also required to manage the manufacturing cost. In this case, the wave amplitude variation becomes an important parameter.

Under the operation of the irregular wave, the LPMGs also suffer losses in load conditions. Whether the component, such as the copper loss, is irregular depends on the load current. Meanwhile, the overall values of the hysteresis and the eddy current losses can be stated based on the maximum flux density. Figure 25 shows the total loss resulted from the two designs under random wave variations. The total loss decreases as the significant wave height and peak frequency increase. Meanwhile, the loss also tends to decrease when the load resistance is increased. The trends of the power losses under several load resistances and random wave configurations are the same for both LPMG designs.

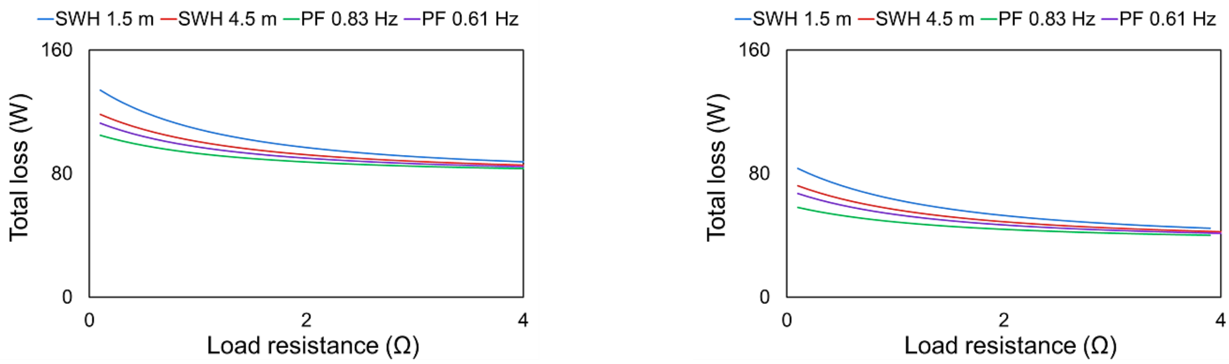

Figure 25. Power loss of iron-cored LPMG (**left**) and semi iron-cored LPMG (**right**) under different random wave parameters and load resistances.

Then, the power loss affects the electrical efficiency of the LPMG. Overall, the electrical efficiency among the same LPMG design is similar under different random wave parameter variations. The trend of the two designs is also identical under the same wave parameter variations. The iron-cored results in electrical efficiencies in the range of 74–75%, while the semi iron-cored results in higher values, around 84% under all random waves. The higher electrical efficiency in the semi iron-cored model, even with higher copper loss, is supported by lower hysteresis and eddy current losses due to the smaller core volume. In Figure 25, the total power loss of the semi iron-cored is lower than the iron-cored. Then, Figure 26 presents the electrical efficiency of the two LPMG models under the same random wave parameter.

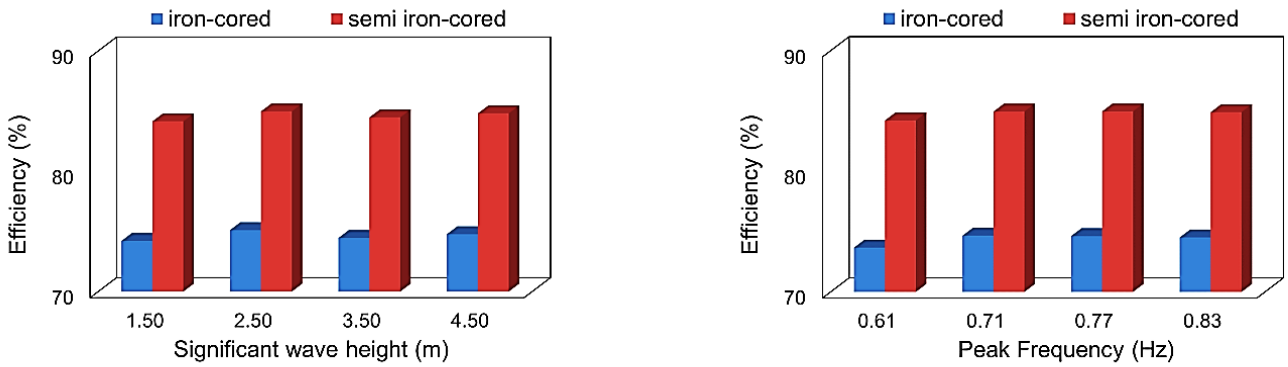

Figure 26. Electrical efficiency of the LPMG designs under random wave configurations.

The resulted efficiencies are also affected by the output power. Under significant wave height variation, the WEC produces output power with the non-specific trend due to the mixed influence from the waves' dynamics. Hence, the efficiency also has no specific trend. Meanwhile, under different peak frequencies, both the output power and total power loss increase as the wave parameter values decrease; thus, the resulted efficiency is also similar under all the parameter values.

Based on the electrical output results, the performance of the semi iron-cored LPMG is better in terms of power loss and electrical efficiency. For direct-drive WEC with a similar LPMG design (but with optimized dimensions), the obtained results can also be a consideration for selecting the placement location. Under unidirectional long-crested random wave scenarios with similar significant wave height, it is preferred to install the WEC in sites with lower peak frequency. It is favored, since the output power and efficiency will be higher, whereas the power loss will be smaller.

The advancement of this research in future work besides optimizing the LPMG dimensions is regarding the experiment for testing. The aim is to more approach real wave situations. The focus will still be on the same placement location, since the basic design and the wave height data are available. However, to move the translator according to the complete random wave dynamics is quite a challenge. It will be easier to take a portion of the random wave motion, which is composed of several regular waves. Then, each regular wave with certain parameters' values (amplitude and frequency) can be taken as an input to experimentally move the translator at a time. The outputs are next combined to form the complete output of a random wave motion part.

4. Conclusions

Unidirectional long-crested random waves have been generated to test a direct-drive WEC with two LPMG options. Four different significant wave heights and four different peak frequencies are used based on the real data in the Southern Coast of Yogyakarta, Indonesia, which is the designated place for the 1 kW-rated WEC. After being analyzed using the JONSWAP energy spectrum, the wave's particle elevation graphs can be obtained, from which the operation of the WEC system (floater and LPMG) can be simulated. An experiment is also conducted to check the output of the real LPMG models. In this case, the small-scale LPMG models (about one-third in dimensions) produce similar output trends as the theoretical ones for a constant translation speed of 1 m/s. The resulted voltages from both real LPMGs are about one-seventh of the theoretical values.

Two factors shape the LPMGs' output power under the tested random waves. First, the accommodation of the high waves from the ocean data results in non-facing events, which reduce the overall voltage and power. Second, the shorter dimension of the LPMG compared to the wave amplitude makes it difficult to harness high speed during optimum position. Related to the second factor, the high translation speeds from the wave's mechanisms do not always result in high voltage, because it also depends on the translator-stator position.

Analyzing the outputs of both LPMGs, the resulted powers under significant wave height variation are higher than from peak frequency variation. Furthermore, the output powers from different significant wave heights have no specific trend, as it is affected negatively by the non-facing event frequency and positively by the higher average translation speed. Meanwhile, the peak frequency is inversely proportional to the output power, as it is also inversely proportional to the average translation speed and JONSWAP energy spectrum. The non-facing event is similar among different peak frequencies, so the effect is not significant. If the non-facing events are expelled, the output power increases, with the increase rising as the significant wave height increases. This is because the non-facing event frequency is linearly proportional to the significant wave height. For different peak frequencies, the output power increase is similar and insignificant.

The iron-cored LPMG produces higher power than the semi iron-cored type, due to its lower winding impedance. Meanwhile, for both designs, the resulted power losses are inversely proportional to the significant wave height or the peak frequency values. The loss also has negative relation with the load resistance value. Furthermore, the resulted efficiencies among different wave parameters' values are similar for the same LPMG design, with semi iron-cored LPMG producing higher efficiency due to its lower hysteresis and eddy current losses.

From the performance test results, the semi iron-cored LPMG is preferred in terms of power loss and electrical efficiency. Meanwhile, for a similar LMPG design (iron-cored or semi iron-cored type), it is preferred to select the placement location with a lower peak frequency wave for equal significant wave height.

This research only focuses on the provided LPMGs with a nearly equal length between the stator and the translator, and the effective translator stroke (to effectively produce electrical output) is shorter than the wave amplitudes. From the results, the designs have not met the expected output, even after the non-facing events are excluded. For improvement, the dimensions' extension should be investigated to optimize both output power and manufacturing cost in a minimum possible dimension. The experiment in future research will also be developed by moving the translator according to different regular waves, which are composing a portion of random wave motion.

Author Contributions: Conceptualization, B.A., E.Y. and F.D.W.; methodology, B.A. and E.Y.; software, B.A. and E.Y.; validation, B.A., E.Y. and F.D.W.; formal analysis, B.A.; investigation, B.A.; resources, B.A.; writing—original draft preparation, B.A. and E.Y.; writing—review and editing, E.Y. and F.D.W.; visualization, B.A.; supervision, E.Y. and F.D.W.; project administration, E.Y. and F.D.W. All authors have read and agreed to the published version of the manuscript.

Funding: This research received no external funding.

Acknowledgments: The authors would like to acknowledge the Research Center for Electrical Power and Mechatronics (RCEPM), Indonesian Institute of Sciences (LIPI), and Universitas Gadjah Mada-Indonesia for the support and facilities provided in conducting this research.

Conflicts of Interest: The authors declare no conflict of interest.

References

1. Farrok, O.; Ahmed, K.; Tahlil, A.D.; Farah, M.M.; Kiran, M.R.; Islam, R. Electrical Power Generation from the Oceanic Wave for Sustainable Advancement in Renewable Energy Technologies. *Sustainability* **2020**, *12*, 2178. [CrossRef]
2. Farrok, O.; Islam, R.; Sheikh, M.R.I.; Guo, Y.G.; Zhu, J.G. Design and Analysis of a Novel Lightweight Translator Permanent Magnet Linear Generator for Oceanic Wave Energy Conversion. *IEEE Trans. Magn.* **2017**, *53*, 1–4. [CrossRef]
3. Wahyudie, A.; Susilo, T.B.; Jehangir, S.S. Design of a 100 W mini permanent magnet linear generator for wave energy converter system. In Proceedings of the 2018 5th International Conference on Renewable Energy: Generation and Applications, Rome, Italy, 24–26 September 2018; pp. 223–226. [CrossRef]

4. Doyle, S.; Aggidis, G.A. Development of multi-oscillating water columns as wave energy converters. *Renew. Sustain. Energy Rev.* **2019**, *107*, 75–86. [CrossRef]
5. Widén, J.; Munkhammar, J. *Solar Radiation Theory*; Uppsala University: Uppsala, Sweden, 2019. [CrossRef]
6. Musolino, A.; Rizzo, R.; Sani, L.; Mattiazzo, G.; Vissio, G.; Bracco, G. Double and single sided tubular linear Permanent Magnets generator for the Wave Energy conversion. In Proceedings of the 2016 AEIT International Annual Conference (AEIT), Capri, Italy, 3–5 August 2016; pp. 1–6. [CrossRef]
7. Ocean Energy Europe. Ocean Energy Key Trends and Statistics 2019. 2020. Available online: https://www.oceanenergy-europe.eu/wp-content/uploads/2020/03/OEE_Trends-Stats_2019_Web.pdf (accessed on 2 April 2021).
8. Qiu, S.; Liu, K.; Wang, D.; Ye, J.; Liang, F. A comprehensive review of ocean wave energy research and development in China. *Renew. Sustain. Energy Rev.* **2019**, *113*, 109271. [CrossRef]
9. Ocean Energy Systems. Annual Report Ocean Energy Systems 2016. 2017. Available online: https://report2016.ocean-energy-systems.org/ (accessed on 11 March 2018).
10. Satriawan, M.; Liliasari, L.; Setiawan, W.; Abdullah, A.G. Unlimited Energy Source: A Review of Ocean Wave Energy Utilization and Its Impact on the Environment. *Indones. J. Sci. Technol.* **2021**, *6*, 1–16. [CrossRef]
11. Kurniawan, R.; Khotimah, M.K. Ocean Wave Characteristics in Indonesian Waters for Sea Transportation Safety and Planning. *IPTEK J. Technol. Sci.* **2016**, *26*. [CrossRef]
12. BPPT. Indonesia Energy Outlook 2018: Sustainable Energy for Land Transportation. 2019. Available online: https://www.bppt.go.id/outlook-energi/bppt-outlook-energi-indonesia-2018/download (accessed on 10 June 2019).
13. Indonesia Ministry of Energy and Mineral Resources (ESDMK); Ketenagalistrikan, D. Statistik Ketenaga Listrikan Tahun 2018. 2019. Available online: https://gatrik.esdm.go.id/assets/uploads/download_index/files/92999-statistik-2018.pdf (accessed on 1 December 2020).
14. Sugianto, D.N.; Kunarso, M.; Helmi, L.; Maslukah, I.; Alifdini, S.; Saputro, M.; Yusuf, E.; Endrawati, H. Wave Energy Reviews in Indonesia. *IJMET* **2017**, *8*, 13.
15. Rizal, A.M.; Ningsih, N.S. Ocean wave energy potential along the west coast of the Sumatra island, Indonesia. *J. Ocean Eng. Mar. Energy* **2020**, *6*, 137–154. [CrossRef]
16. Faulincia, F. Studi Potensi Pembangkit Listrik Tenaga Gelombang Laut Dengan Metoda Oscilating Water Column Di Perairan Kendari Indonesia. *J. Mech. Eng. Mechatronics* **2019**, *4*, 7–14. [CrossRef]
17. Mulkan, A.; Zulfadli, T. Studi Awal Energi Gelombang Laut Di Perairan Bireuen Sebagai Sumber Pembangkit Listrik. *J. Geuthee Penelit. Multidisiplin* **2018**, *1*, 7.
18. Safitri, L.E.; Jumarang, M.I.; Apriansyah, A. Studi Potensi Energi Listrik Tenaga Gelombang Laut Sistem Oscillating Water Column (OWC) di Perairan Pesisir Kalimantan Barat. *Positron* **2016**, *6*. [CrossRef]
19. Wu, Z.; Viola, A. The challenge of wave energy: A review of the WECs state of the art developed in the world. *Oceans* **2017**, 1–6. [CrossRef]
20. Hong, Y.; Temiz, I.; Pan, J.; Eriksson, M.; Boström, C. Damping Studies on PMLG-Based Wave Energy Converter under Oceanic Wave Climates. *Energies* **2021**, *14*, 920. [CrossRef]
21. Wave Energy: Technology brief. IRENA Ocean Energy Technology Brief 4. 2014. Available online: https://www.irena.org/publications/2014/Jun/Wave-energy/ (accessed on 27 June 2021).
22. Qiao, D.; Haider, R.; Yan, J.; Ning, D.; Li, B. Review of Wave Energy Converter and Design of Mooring System. *Sustainability* **2020**, *12*, 8251. [CrossRef]
23. Orphin, J.; Fleming, A.; Algie, C. Physical scale model testing of a flexible membrane wave energy converter: Videogrammetric analysis of membrane operation. *Int. J. Mar. Energy* **2017**, *20*, 135–150. [CrossRef]
24. Badan Pengkajian dan Penerapan Teknologi (BPPT) Republik Indonesia. Available online: https://www.bppt.go.id/index.php/profil/organisasi/607-dorong-pemanfaatan-energi-terbarukan-di-masyarakat. (accessed on 12 December 2016).
25. International Renewable Energy Agency (IRENA). *Ocean Energy: Technologies, Patents, Deployment Status and Outlook*; IRENA: Abu Dhabi, UAE, 2014.
26. Kofoed, P.; Pecher, A. *Handbook of Ocean Wave Energy*, 1st ed.; Springer International Publishing: Cham, Switzerland, 2017. [CrossRef]
27. Handoko, C.; Mukhtasor, P. The development of power take-off technology in wave energy converter systems: A Review. *IOP Conf. Ser. Earth Environ. Sci.* **2021**, *739*, 12081. [CrossRef]
28. Drew, B.; Plummer, A.; Sahinkaya, M. A review of wave energy converter technology. *Proc. Inst. Mech. Eng. Part A J. Power Energy* **2009**, *223*, 887–902. [CrossRef]
29. Hamim, M.A.F.M.; Ibrahim, T.; Nor, N.M. Modeling and analyze a single-phase halbach magnetized tubular linear permanent magnet generator for wave energy conversion. In Proceedings of the 2014 IEEE International Conference on Power and Energy (PECon), Kuching, Malaysia, 3–6 December 2014; pp. 87–92. [CrossRef]
30. Huang, L.; Hu, M.; Chen, Z.; Yu, H.; Liu, C. Research on a Direct-Drive Wave Energy Converter Using an Outer-PM Linear Tubular Generator. *IEEE Trans. Magn.* **2017**, *53*, 1–4. [CrossRef]

31. Bode, C.; Schillingmann, H.; Henke, M. A free-piston PM linear generator in vernier topology using quasi-Halbach-excitation. In Proceedings of the 2014 International Conference on Electrical Machines (ICEM), Berlin, Germany, 3–8 September 2014; pp. 1950–1955. [CrossRef]
32. Faiad, A.A.; Gowaid, I.A. Linear generator technologies for wave energy conversion applications: A review. In Proceedings of the 2018 53rd International Universities Power Engineering Conference (UPEC), Glasgow, UK, 17–19 July 2018; pp. 1–6. [CrossRef]
33. Khatri, P.; Wang, X. Comprehensive review of a linear electrical generator for ocean wave energy conversion. *IET Renew. Power Gener.* **2020**, *14*, 949–958. [CrossRef]
34. Ridge, A.; Clifton, P.; McMahon, R.; Kelly, H.-P. Force ripple compensation in a tubular linear generator for marine renewable generation. In Proceedings of the 2011 IEEE International Electric Machines & Drives Conference (IEMDC), Niagara Falls, ON, Canada, 8–11 May 2011; pp. 480–485. [CrossRef]
35. Hamim, M.A.F.M.; Ibrahim, T.; Nor, N.M.; Makamper, M.H. Modeling of a tubular permanent magnet linear generator for wave energy conversion using finite element method. In Proceedings of the 2014 5th International Conference on Intelligent and Advanced Systems (ICIAS), Kuala Lumpur, Malaysia, 20–23 June 2014; pp. 1–5. [CrossRef]
36. Huang, L.; Yu, H.; Hu, M.; Liu, C.; Yuan, B. Research on a Tubular Primary Permanent-Magnet Linear Generator for Wave Energy Conversions. *IEEE Trans. Magn.* **2013**, *49*, 1917–1920. [CrossRef]
37. Memon, A.H.; Bin Ibrahim, T.; Perumal, N. Portable and pico-scale linear generator for wave energy conversion. In Proceedings of the 2014 5th International Conference on Intelligent and Advanced Systems (ICIAS), Kuala Lumpur, Malaysia, 10–15 June 2014; pp. 1–4. [CrossRef]
38. Ibrahim, T.; Hussain, A.; Nallagowden, P.; Abrro, F.R. Design development and modelling of linear permanent magnet generator topologies for wave energy conversion. *Int. J. Appl. Eng. Res.* **2017**, *12*, 3329–3336.
39. Oprea, C.A.; Martis, C.S.; Jurca, F.; Fodorean, D.; Szabo, L. Permanent magnet linear generator for renewable energy applications: Tubular vs. four-sided structures. In Proceedings of the 2011 International Conference on Clean Electrical Power (ICCEP), Ischia, Italy, 20–25 June 2011; pp. 588–592. [CrossRef]
40. Vermaak, R.; Kamper, M.J. Design Aspects of a Novel Topology Air-Cored Permanent Magnet Linear Generator for Direct Drive Wave Energy Converters. *IEEE Trans. Ind. Electron.* **2011**, *59*, 2104–2115. [CrossRef]
41. Brovont, A.; Pekarek, S.D. Modeling air-core permanent-magnet linear generators in free-rotating devices. In Proceedings of the 2015 IEEE International Electric Machines & Drives Conference (IEMDC), Coeur D'Alene, ID, USA, 18–23 May 2015; pp. 735–741. [CrossRef]
42. Wijaya, F.D.; Azhari, B.; Sarjiya, S. Simulation of modified tubular linear permanent magnet generator for wave energy conversion in Indonesia. In Proceedings of the 2017 3rd International Conference on Science and Technology Computer (ICST), Yogyakarta, Indonesia, 7–11 July 2017; pp. 39–44. [CrossRef]
43. Sugita, M.R.P.; Wijaya, F.D.; Sarjiya, S. Design and analysis of tri core permanent magnet linear generator for wave energy conversion in south coast of Java Island. In Proceedings of the 2016 6th International Annual Engineering Seminar (InAES), Yogyakarta, Indonesia, 3–8 August 2016; pp. 256–261. [CrossRef]
44. Azhari, B.; Yazid, E. Performance of Wave Energy Converter using Linear Permanent Magnet Generator under Regular Wave Condition. In Proceedings of the 2019 International Conference on Sustainable Energy Engineering and Application (ICSEEA), Tangerang, Indonesia, 4–10 October 2019; pp. 56–61. [CrossRef]
45. Brekken, T. Fundamentals of ocean wave energy conversion, modeling, and control. In Proceedings of the 2010 IEEE International Symposium on Industrial Electronics, Bari, Italy, 10–14 July 2010; pp. 3921–3966. [CrossRef]
46. Kim, J.-M.; Koo, M.-M.; Jeong, J.-H.; Hong, K.; Cho, I.-H.; Choi, J.-Y. Design and analysis of tubular permanent magnet linear generator for small-scale wave energy converter. *AIP Adv.* **2017**, *7*, 56630. [CrossRef]
47. Irhas, O.; Suryaningsih, R. Study on Wave Energy into Electricity in the South Coast of Yogyakarta, Indonesia. *Energy Procedia* **2014**, *47*, 149–155. [CrossRef]
48. Kurniawan, R.; Habibie, M.N.; Suratno, S. Variasi Bulanan Gelombang Laut di Indonesia. *JMG* **2011**, *12*. [CrossRef]
49. Prendergast, J.; Li, M.; Sheng, W. A Study on the Effects of Wave Spectra on Wave Energy Conversions. *IEEE J. Ocean. Eng.* **2020**, *45*, 271–283. [CrossRef]
50. Nair, M.A.; Kumar, V.S. Wave spectral shapes in the coastal waters based on measured data off Karwar on the western coast of India. *Ocean Sci.* **2017**, *13*, 365–378. [CrossRef]
51. Montasir, O.; Kurian, V. Effect of slowly varying drift forces on the motion characteristics of truss spar platforms. *Ocean Eng.* **2011**, *38*, 1417–1429. [CrossRef]
52. Son, S. Design of Ocean Platforms Against Ringing Response. Master' Thesis, Science in Mechanical Engineering, Graduate Faculty of Texas Tech University, Lubbock, TX, USA, 2006.
53. Cummins, W.E. The Impulse Response Function and Ship Motions. *David Taylor Model Basin*. 1962. Available online: http://hdl.handle.net/1721.3/49049 (accessed on 30 March 2020).
54. Fossen, T.I.; Perez, T. Marine Systems Simulator (MSS). 2004. Available online: http://www.msstoolbox.org (accessed on 5 March 2020).
55. Sinnadurai, R.; Ting, C.; Zani, N.H.M. Analysis and optimization of a three phase linear generator using Finite Element Method Magnetics (FEMM). In Proceedings of the 2016 IEEE Student Conference on Research and Development (SCOReD), Kuala Lumpur, Malaysia, 4–9 December 2016; pp. 1–6. [CrossRef]

56. Boldea, I. *Linear Electric Machines, Drives, and MAGLEVs Handbook*; CRC Press: Boca Raton, FL, USA, 2013.
57. Pirisi, A.; Gruosso, G.; Zich, R.E. Novel Modeling Design of Three Phase Tubular Permanent Magnet Linear Generator for Marine Applications. In Proceedings of the International Conference on Power Engineering, Energy and Electrical Drives, Lisbon, Portugal, 18–20 March 2009; pp. 78–83. [CrossRef]
58. Kimoulakis, N.; Kakosimos, P.; Kladas, A. Power generation by using point absorber wave energy converter coupled with linear permanent magnet generator. In Proceedings of the 7th Mediterranean Conference and Exhibition on Power Generation, Transmission, Distribution and Energy Conversion (MedPower 2010), Agya Napa, Cyprus, 7–10 November 2010; p. 214. [CrossRef]